

Sketch Tomography: Hybridizing Classical Shadow and Matrix Product State

Xun Tang^{1*}, Haoxuan Chen², Yuehaw Khoo^{3,4}, Lexing Ying^{1,2}

¹Department of Mathematics, Stanford University, Stanford, CA, 94305, USA.

²Institute for Computational and Mathematical Engineering (ICME), Stanford University, Stanford, CA, 94305, USA.

³Department of Statistics, University of Chicago, Chicago, IL, 60637, USA.

⁴Committee on Computational and Applied Mathematics (CCAM), University of Chicago, Chicago, IL, 60637, USA.

*Corresponding author(s). E-mail(s): xuntang@stanford.edu;
Contributing authors: haoxuanc@stanford.edu; ykhoo@uchicago.edu;
lexing@stanford.edu;

Abstract

We introduce Sketch Tomography, an efficient procedure for quantum state tomography based on the classical shadow protocol used for quantum observable estimations. The procedure applies to the case where the ground truth quantum state is a matrix product state (MPS). The density matrix of the ground truth state admits a tensor train ansatz as a result of the MPS assumption, and we estimate the tensor components of the ansatz through a series of observable estimations, thus outputting an approximation of the density matrix. The procedure is provably convergent with a sample complexity that scales quadratically in the system size. We conduct extensive numerical experiments to show that the procedure outputs an accurate approximation to the quantum state. For observable estimation tasks involving moderately large subsystems, we show that our procedure gives rise to a more accurate estimation than the classical shadow protocol. We also show that sketch tomography is more accurate in observable estimation than quantum states trained from the maximum likelihood estimation formulation.

Keywords: Quantum state tomography, Classical shadow, Low-rank methods

1 Introduction

Quantum state tomography (QST) is a crucial part of quantum computing for verifying the output of quantum algorithms and quantum devices [1–4]. This work considers a broad class of QST tasks where the ground truth quantum state $|\psi\rangle$ admits a matrix product state (MPS) representation [5]. The MPS ansatz is a special 1D tensor network characterized by limited entanglements between sites. For example, the MPS ansatz can represent qubits entangled by shallow local quantum circuits [6].

We introduce Sketch Tomography, a sketching-based tomography procedure that recovers the density matrix ρ of $|\psi\rangle$ through classical shadow. The MPS assumption on $|\psi\rangle$ implies ρ is representable by a tensor train (TT). The classical shadow protocol [7] provides a density matrix approximation $\hat{\rho} \approx \rho$. Our sketching procedure uses $\hat{\rho}$ to output a TT approximation $\tilde{\rho} \approx \rho$. For global observables, using $\tilde{\rho}$ for observable estimation is more accurate than using $\hat{\rho}$.

Essentially, sketch tomography is a procedure that conducts observable estimation to approximate each tensor component in the TT representation of ρ . Those tensor components can be obtained by solving linear equations formed from observable estimations on ρ . Thus, we use $\hat{\rho}$ from classical shadow to formulate approximate linear equations, and solving these linear equations leads to a TT approximation $\tilde{\rho} \approx \rho$. Our procedure only involves postprocessing of $\hat{\rho}$ and can be carried out classically.

After the procedure is carried out, the output $\tilde{\rho}$ can be used for observable estimation. For global observables, we show empirically that using our tensor train approximation for observable estimation leads to a higher accuracy when compared with the estimate obtained by classical shadow under random Pauli measurements. The underlying cause of the improved accuracy is that $\tilde{\rho}$ provably approximates ρ in the Frobenius norm. As a result, $\tilde{\rho}$ can accurately perform observable estimation for generic observables O , whereas the classical shadow estimation has a large variance for global observables. In addition, the output $\tilde{\rho}$ also allows for other prediction tasks such as entanglement entropy prediction.

Several prior works on QST have considered the MPS ansatz. We include a detailed discussion on related work in Appendix A. Our work bears the most resemblance to [3, 8], where a direct tomography procedure measures the local density matrices to reconstruct the tensor network structure of the full density matrix. Our work essentially improves on this approach by obtaining the tensor components from general sketches that are not necessarily the local density matrix. As a result, our proposal allows direct tomography procedures to handle systems with non-local interactions. Moreover, as we form the sketches from classical shadows, our proposal does not require direct access to copies of ρ .

2 Procedure

Throughout this text, we focus on the setting of n -qubit systems. We assume that $|\psi\rangle \in \mathbb{C}^{2^n}$ is a fixed but unknown target quantum state, and $\rho \in \mathbb{C}^{2^n \times 2^n}$ is its corresponding density matrix. The goal is to approximate ρ accurately. We go through the main idea of the procedure for sketch tomography, and equations are primarily illustrated with tensor diagrams. The derivation and implementation details can be

found in Appendix C. For an integer $n > 0$, we write $[n] := \{1, \dots, n\}$. For $k < n$, we write $[n] - [k] = \{k+1, \dots, n\}$, where the $-$ symbol denotes set difference.

The procedure requires access to the output of the classical shadow protocol [7]. Through repeated random Pauli measurements, the protocol outputs a collection of W approximations $\hat{\rho}_1, \dots, \hat{\rho}_W$ and uses a median-of-means estimator [9] for observable estimation. For simplicity, we illustrate the procedure with $W = 1$ so that there is only one approximation $\hat{\rho} \approx \rho$.¹

We go through our QST procedure for obtaining ρ . For $k \in [n]$, we let $(\sigma_k^X, \sigma_k^Y, \sigma_k^Z)$ denote the Pauli matrices on site k , and we write $(\sigma_k^1, \sigma_k^2, \sigma_k^3, \sigma_k^4) = (\frac{1}{\sqrt{2}}I_2, \frac{1}{\sqrt{2}}\sigma_k^X, \frac{1}{\sqrt{2}}\sigma_k^Y, \frac{1}{\sqrt{2}}\sigma_k^Z)$. A density matrix ρ can be uniquely represented by a tensor $C: [4]^n \rightarrow \mathbb{R}$ as follows:

$$\rho = \sum_{i_1, \dots, i_n=1}^4 C(i_1, \dots, i_n) \prod_{l=1}^n \sigma_l^{i_l}. \quad (1)$$

In particular, the MPS assumption of $|\psi\rangle$ implies that C is a tensor train (TT). One represents C in a tensor diagram as follows:

$$\begin{array}{c} \boxed{C} \\ \text{\scriptsize } i_1 \quad i_2 \quad \dots \quad i_n \end{array} = \begin{array}{c} \boxed{G_1} \text{---} \boxed{G_2} \text{---} \dots \text{---} \boxed{G_n} \\ \text{\scriptsize } i_1 \quad i_2 \quad \quad \quad i_n \end{array}. \quad (2)$$

Intuitively, our procedure utilizes the TT structure of ρ and uses the noisy copy $\hat{\rho}$ from classical shadow to recover ρ . As shown in Equation (2), C is defined in terms of tensor components $(G_k)_{k=1}^n$.

We illustrate how we obtain each G_k for a fixed site k . First, we rewrite Equation (2) as a linear equation for G_k . We define two tensors $C_{<k}, C_{>k}$ by the following diagram

$$\begin{array}{c} \boxed{C_{<k}} \\ \text{\scriptsize } i_1 \quad \dots \quad i_{k-1} \end{array} \text{---} = \begin{array}{c} \boxed{G_1} \text{---} \dots \text{---} \boxed{G_{k-1}} \\ \text{\scriptsize } i_1 \quad \quad \quad i_{k-1} \end{array}, \quad \text{---} \begin{array}{c} \boxed{C_{>k}} \\ \text{\scriptsize } i_{k+1} \quad \dots \quad i_n \end{array} = \text{---} \begin{array}{c} \boxed{G_{k+1}} \text{---} \dots \text{---} \boxed{G_n} \\ \text{\scriptsize } i_{k+1} \quad \quad \quad i_n \end{array}, \quad (3)$$

and the equation for G_k is written as follows:

$$\begin{array}{c} \boxed{C_{<k}} \text{---} \boxed{G_k} \text{---} \boxed{C_{>k}} \\ \text{\scriptsize } i_1 \quad \dots \quad i_{k-1} \quad i_k \quad i_{k+1} \quad \dots \quad i_n \end{array} = \begin{array}{c} \boxed{C} \\ \text{\scriptsize } i_1 \quad i_2 \quad \dots \quad i_n \end{array}. \quad (4)$$

The linear system in Equation (4) is over-determined and is impractical to solve when n is large. To obtain a practical linear system, we employ sketch tensors $S_{<k} =$

$$\begin{array}{c} \boxed{S_{<k}} \\ \text{\scriptsize } i_1 \quad \dots \quad i_{k-1} \\ \text{\scriptsize } \zeta \end{array}, \quad S_{>k} = \begin{array}{c} \boxed{S_{>k}} \\ \text{\scriptsize } i_{k+1} \quad \dots \quad i_n \\ \text{\scriptsize } \mu \end{array}. \quad \text{We obtain the desired equation for } G_k \text{ by contracting}$$

¹Given $\hat{\rho}_1, \dots, \hat{\rho}_W$, one clear alternative is to simply use $\hat{\rho} = \frac{1}{W} \sum_{i=1}^W \hat{\rho}_i$, and using $\hat{\rho}$ for observable estimation is called the direct mean approach. Our numerical tests find that the direct mean approach has similar performance compared with the median of means, and a similar conclusion was also reported in [10].

Equation (4) with $S_{<k}$ and $S_{>k}$:

Diagram (5) illustrates the contraction of tensors. On the left, a box labeled $C_{<k}$ is connected to a box labeled G_k , which is connected to a box labeled $C_{>k}$. Below $C_{<k}$ is a box labeled $S_{<k}$ with multiple vertical lines connecting them. Below $C_{>k}$ is a box labeled $S_{>k}$ with multiple vertical lines connecting them. The index i_k is shown between G_k and $S_{>k}$, and μ is shown below $S_{>k}$. This is set equal to a single box labeled C on the right. Below C are two boxes, $S_{<k}$ and $S_{>k}$, each with multiple vertical lines connecting them to C . The index i_k is shown between these two boxes, and ζ is shown below $S_{<k}$, while μ is shown below $S_{>k}$.

Simplifying Equation (5), we get

Diagram (6) shows the simplified equation. On the left, a box labeled $A_{<k}$ is connected to a box labeled G_k , which is connected to a box labeled $A_{>k}$. Below $A_{<k}$ is the index ζ , below G_k is the index i_k , and below $A_{>k}$ is the index μ . This is set equal to a single box labeled B_k on the right. Below B_k are the indices ζ , i_k , and μ .

where $A_{>k}, A_{<k}$ are respectively the contraction of $C_{>k}, C_{<k}$ by $S_{>k}, S_{<k}$, and B_k is the contraction of C by $S_{>k} \otimes S_{<k}$.

To obtain G_k , we use $\hat{\rho}$ to approximate all terms in Equation (6). Obtaining B_k is straightforward. We note from Equation (5) that B_k is a linear measurement of C . By Equation (1), one can see that each entry of B_k is an observable of ρ . Therefore, using $\hat{\rho}$ allows one to approximately obtain B_k .

To obtain $A_{>k}, A_{<k}$, we suppose that the sketch tensor $S_{>j}, S_{<j}$ has been defined for all j . The tensors $C_{>j}, C_{<j}$ are defined according to Equation (3), and $A_{>j}, A_{<j}$ are defined accordingly. We let Z_k be the contraction of C by $S_{<(k+1)} \otimes S_{>k}$. To get $A_{>k}$, we use the following equation for Z_k :

Diagram (7) shows the equation for Z_k . On the left, a box labeled $A_{<(k+1)}$ is connected to a box labeled $A_{>k}$. Below $A_{<(k+1)}$ is a vertical line, and below $A_{>k}$ is a vertical line. This is set equal to Z_k , which is then set equal to a box labeled C on the right. Below C are two boxes, $S_{<(k+1)}$ and $S_{>k}$, each with multiple vertical lines connecting them to C . Below $S_{<(k+1)}$ is a vertical line, and below $S_{>k}$ is a vertical line.

where the first equality is by the definition of $A_{<(k+1)}, A_{>k}$. The only requirement for determining $(A_{<(k+1)}, A_{>k})$ is that the first equality in Equation (7) needs to hold. Therefore, to obtain $A_{>k}$, we use $\hat{\rho}$ to approximately obtain Z_k . Then, we perform a truncated SVD on Z_k and we set $(A_{<(k+1)}, A_{>k})$ to be the best low-rank approximation of Z_k . One can similarly obtain $A_{<k}$ by approximating Z_{k-1} and performing a truncated SVD.

Therefore, approximately obtaining $A_{<k}, A_{>k}, B_k$ for all k allows one to solve for all G_k . Let $(\hat{G}_k)_{k=1}^n$ be the approximated tensor component obtained from the procedure. The output $\tilde{\rho}$ is defined as follows:

$$\tilde{\rho} = \sum_{i_{[n]} \in [4]^n} \sum_{\alpha_1, \dots, \alpha_{n-1}} \hat{G}_1(i_1, \alpha_1) \hat{G}_2(\alpha_1, i_2, \alpha_2) \cdots \hat{G}_n(\alpha_{n-1}, i_n) \prod_{l=1}^n \sigma_l^{i_l}. \quad (8)$$

2.1 Performance guarantee

The sketch tomography output $\tilde{\rho}$ converges to ρ in the Frobenius norm. We present an informal version below, but we note that the formal version is a non-asymptotic convergence bound:

Proposition 1 (*Informal version of the upper bound*) *Let ρ be the density matrix of a matrix product state for n qubits with n sufficiently large. Let $\tilde{\rho}$ denote the output of the sketch tomography procedure, and suppose the observable estimations are done using the classical shadow protocol from B random Pauli measurements. Let $\varepsilon, \delta \in (0, 1)$ be accuracy parameters. A sample size of $B \geq \mathcal{O}(n^2 \log(n/\delta) \varepsilon^{-2})$ ensures that $\|\rho - \tilde{\rho}\|_F < \varepsilon$ with probability $1 - \delta$.*

In particular, the guarantee in Theorem 1 means that $\tilde{\rho}$ obtained from sketch tomography enjoys an accurate approximation on global observables regardless of whether the observable O is a local observable. We further corroborate the accuracy of $\tilde{\rho}$ in observable estimation tasks by the numerical experiments in Section 3. For the formal version of Theorem 1, and the proof, we refer the readers to Appendix D.

2.2 Information-theoretical lower bound

We further provide a lower bound on the required number of measurements in the proposition below, which serves as a complement to the performance guarantee presented in Theorem 1 above.

Proposition 2 (*Informal version of the lower bound*) *Consider the setting of estimating a quantum state by using the classical shadow protocol based on random Pauli measurements. For a given error tolerance ε , there exists some matrix product state with density matrix ρ , such that it requires at least (order) $\frac{n}{\varepsilon^2}$ measurements to obtain an estimator $\tilde{\rho}$ of ρ satisfying $\|\tilde{\rho} - \rho\|_F \leq \varepsilon$.*

We note that the lower bound presented above, which is mainly derived from an information-theoretic perspective, depends primarily on the expressive richness of the tensor-train class and the fundamental limitations on the efficiency of the classical shadow protocol. For a formal version of Theorem 2 and a complete proof, we refer the readers to Appendix F below.

For the sample complexity, we remark that Theorem 2 notably has only a linear dependence on n , the number of qubits, whereas Theorem 1 has a quadratic dependence on n . We conjecture that using $\tilde{\rho}$ as a warm start for tensor network training leads to a better dependence on n .

3 Numerical Experiments

We run three challenging MPS tomography experiments to demonstrate the accuracy of sketch tomography in practice. For the first two examples, we include additional benchmarks by training an MPS model with the maximum likelihood estimation

(MLE) framework on Pauli measurement data, and we also include the trained MLE model as a benchmark. We show that sketch tomography is as accurate as classical shadow in local observable predictions. For global observables, we show that sketch tomography produces a more accurate prediction than classical shadow and the trained MLE model.

3.1 1D Heisenberg

We focus on a 1D antiferromagnetic Heisenberg model with a periodic boundary condition. The Hamiltonian is $H = \sum_{i-i' \equiv 1 \bmod n} (\sigma_i^X \sigma_{i'}^X + \sigma_i^Y \sigma_{i'}^Y + \sigma_i^Z \sigma_{i'}^Z)$. We consider a system with $n = 20$ sites. We use the DMRG implementation in the ITensor package [11] to obtain the ground state $|\psi\rangle$ as an MPS of maximal internal bond dimension $a = 40$. We use the obtained $|\psi\rangle$ as the target state.

We use the tensor train representation of $|\psi\rangle$ to simulate $B = 3 \times 10^5$ random Pauli measurements, and we use the classical shadow protocol to obtain $\hat{\rho}$ for observable estimation. We use sketch tomography to obtain $\tilde{\rho}$. We use the MLE framework to train an MPS model $|\phi\rangle$ on the obtained Pauli measurement data. The training is successful in the sense that $|\phi\rangle$ has a higher likelihood than $|\psi\rangle$ in generating the Pauli measurement data. The detailed methodology for training $|\phi\rangle$ is in Section E.

We test the performance of the considered methods in predicting the two-point correlation function $\langle \vec{\sigma}_1 \cdot \vec{\sigma}_i \rangle := \frac{1}{3} (\langle \sigma_1^X \sigma_i^X \rangle + \langle \sigma_1^Y \sigma_i^Y \rangle + \langle \sigma_1^Z \sigma_i^Z \rangle)$ for $i = 2, \dots, n$. The result is in Figure 1. One can see that $\tilde{\rho}$ is as successful as $\hat{\rho}$ at calculating the two-point correlation function of $|\psi\rangle$.

For global observables, we consider the task of estimating the observable $O_k = \prod_{i=1}^k \sigma_i^X$. One can see that O_k is k -local, and calculating $\langle O_k \rangle$ is known to be challenging for $\hat{\rho}$ when k is large. We plot the result in Figure 2, and we see that both $\tilde{\rho}$ and $|\phi\rangle$ maintain a good accuracy for large k . Moreover, one can see that using the median-of-means estimator has limited benefit to accuracy when k is large.

Lastly, we test the performance of sketch tomography in estimating the entanglement entropy $-\log(\text{tr}[\rho_A^2])$, where A is a subsystem and ρ_A is the partial trace of ρ over all sites not in A . We use $-\log(\text{tr}[\tilde{\rho}_A^2])$ as the sketch tomography prediction, which can be efficiently calculated with tensor diagrams. We test the performance of all possible subsystems A of size at most two, and the result is shown in Figure 3. The maximal prediction error of $\tilde{\rho}$ is 0.010 and the mean prediction error is 0.002, which shows that sketch tomography can accurately predict the entanglement entropy. We also use the MLE output $|\phi\rangle$ for entanglement entropy prediction. We report that the prediction by $|\phi\rangle$ has a larger maximal prediction error of 0.065 and a mean prediction error of 0.004.

3.2 1D TFIM

Our second example focuses on a 1D ferromagnetic transverse field Ising model (TFIM). The Hamiltonian is $H = -J \sum_{i=1}^{n-1} \sigma_i^Z \sigma_{i+1}^Z - J \sigma_1^Z \sigma_n^Z - h \sum_{i=1}^n \sigma_i^X$, where we set $J = h = 1$. We consider a system with $n = 40$ sites. We use DMRG to obtain the ground state $|\psi\rangle$ as an MPS of maximal internal bond dimension $a = 20$.

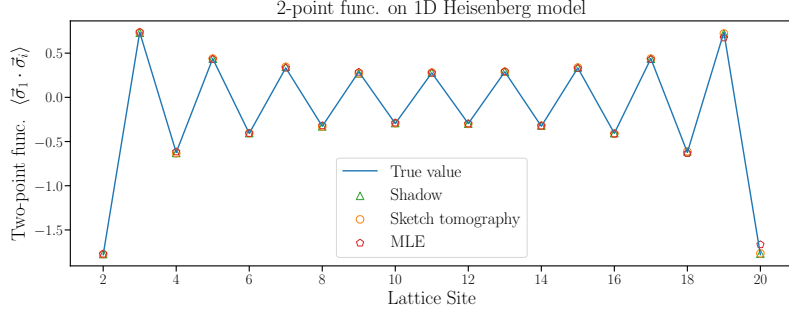


Fig. 1 Predictions of two-point functions $\langle \vec{\sigma}_1 \cdot \vec{\sigma}_i \rangle$ for the ground state of the 1D Heisenberg model with $n = 20$ lattice sites. One can see that sketch tomography reaches a similar accuracy to classical shadow. The prediction from the MLE model is accurate except at the boundary site $i = 20$.

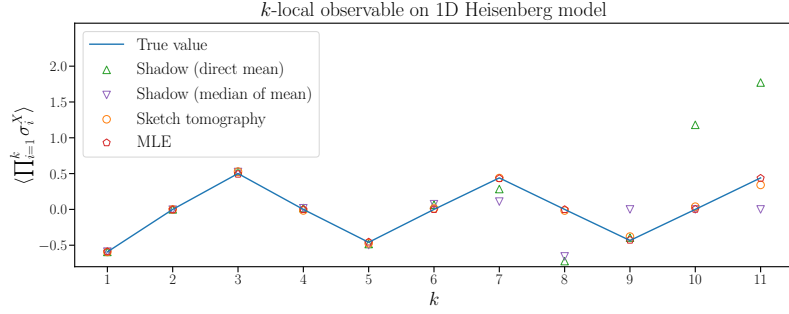


Fig. 2 Predictions of observable $\langle \prod_{i=1}^k \sigma_i^X \rangle$ for the ground state of the 1D Heisenberg model. The median of means version of the classical shadow splits $\hat{\rho}$ into $W = 10$ classical shadow estimators $\hat{\rho}_1, \dots, \hat{\rho}_W$ and reports the median estimation. One can see that using $\hat{\rho}$ from QST for observable estimation is more accurate than using $\hat{\rho}$ from classical shadow.

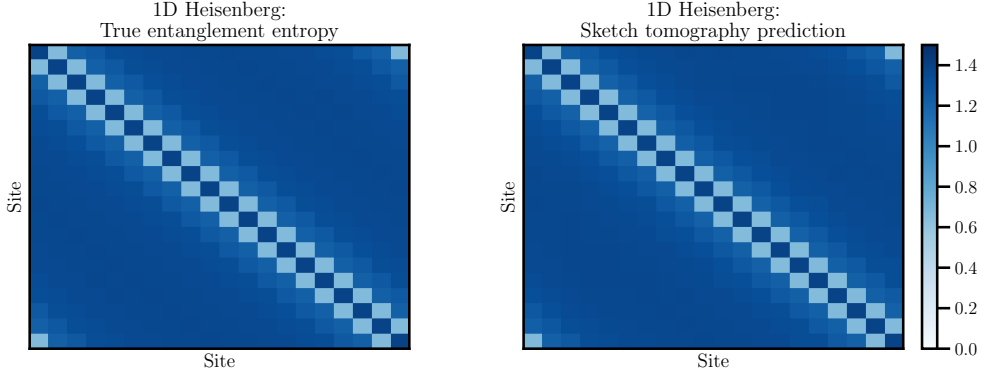


Fig. 3 Prediction of second-order Renyi entanglement entropy for all subsystems of size at most two in the 1D Heisenberg model with $n = 40$ sites. The predicted values using our QST output visually match the true values.

We simulate $B = 3 \times 10^5$ random Pauli measurements on $|\psi\rangle$ and we use the classical shadow protocol to form $\hat{\rho}$ for observable estimation. We apply our sketching-based procedure and obtain $\tilde{\rho}$. We train an MLE model $|\phi\rangle$ on the generated Pauli measurement data. The training detail for $|\phi\rangle$ is in Appendix E. Importantly, the tensor components of $|\phi\rangle$ are of the same size as $|\psi\rangle$, and the training is successful because $|\phi\rangle$ is better than $|\psi\rangle$ in the likelihood metric in MLE.

We test the performance of the methods in predicting the two-point correlation function $\langle \sigma_1^Z \sigma_j^Z \rangle$ for $j = 2, \dots, n$. The result is in Figure 4. One sees that $\tilde{\rho}$ is successful at calculating the two-point correlation function. However, the prediction by the MLE model $|\phi\rangle$ is not accurate. For example, $|\phi\rangle$ does not capture the strong correlation between the boundary sites $(1, n)$.

We consider the observable estimation task over $O_k = \sigma_1^Z \sigma_n^Z \prod_{i=2}^{k-1} \sigma_i^X$ for $k \geq 3$. As in the Heisenberg case, O_k is a k -local observable. The result is in Figure 5. One can see that the prediction from sketch tomography is more accurate than both the classical shadow protocol and the MLE model.

Lastly, we repeat the Renyi entanglement entropy calculation considered in the 1D Heisenberg example. For $\tilde{\rho}$, we report a maximum prediction error of 0.010 and a mean prediction error of 0.003, which shows that sketch tomography is successful in calculating the entanglement entropy in this case. The MLE output $|\phi\rangle$ has a larger maximal prediction error of 0.031, and its mean prediction error is 0.011.

3.3 2D Heisenberg

Our third example focuses on a 2D Heisenberg model with an open boundary condition. The Hamiltonian is $H = \sum_{(i,j) \sim (i',j')} (\sigma_{(i,j)}^X \sigma_{(i',j')}^X + \sigma_{(i,j)}^Y \sigma_{(i',j')}^Y + \sigma_{(i,j)}^Z \sigma_{(i',j')}^Z)$, where $(i, j) \sim (i', j')$ if (i, j) and (i', j') are adjacent on a 8×8 lattice. In this case, the system has $n = 64$ lattice sites. We use the same model as the 2D Heisenberg experiment considered in [7], and we likewise use the ground state data for $|\psi\rangle$ from [12]. The reference ground truth $|\psi\rangle$ is an MPS of maximal internal bond dimension $a = 200$.

The 2D Heisenberg model is significantly more difficult than the other considered cases due to the large parameter size of $|\psi\rangle$. We simulate $B = 8 \times 10^5$ random Pauli measurements on $|\psi\rangle$ and we use the classical shadow protocol to form $\hat{\rho}$. We apply our sketching-based procedure and obtain $\tilde{\rho}$.²

From Figure 6, one can see that our obtained $\tilde{\rho}$ is successful at calculating the two-point correlation function. The mean prediction error of $\tilde{\rho}$ is 0.018, and the mean prediction error of classical shadow is 0.013, which shows that the two methods have comparable performance. The good performance of sketch tomography is noteworthy because representing ρ in a TT ansatz would require an internal bond of $r = a^2 = 40000$, but the obtained $\tilde{\rho}$ only has a maximal internal bond of $r_{\max} = 50$ for computational efficiency considerations.

Lastly, we use $\tilde{\rho}$ to calculate the Renyi entanglement entropy. Similar to the 1D Heisenberg case, we iterate over all subsystems of size at most two, and we show the result in Figure 7. The maximal prediction error is substantially larger at 0.210, but

²We do not provide the training results for MLE because the true MPS model has approximately 5×10^6 parameters, which is significantly larger than the sample size. Thus, the comparison with MLE would be inconclusive due to concerns regarding overfitting.

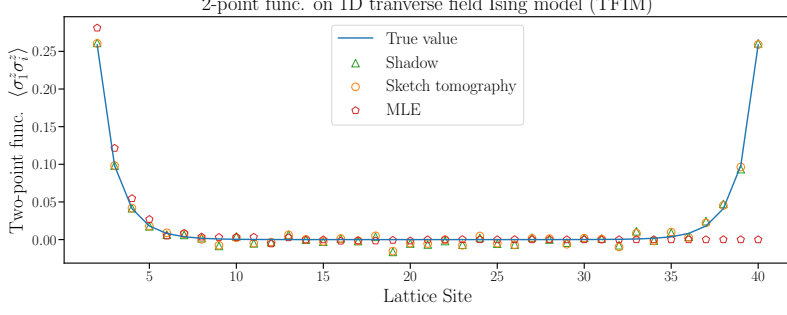


Fig. 4 Predictions of two-point functions $\langle \sigma_1^Z \sigma_i^Z \rangle$ for the ground state of the 1D TFIM model with $n = 40$ lattice sites. One can see that sketch tomography reaches the accuracy of classical shadow.

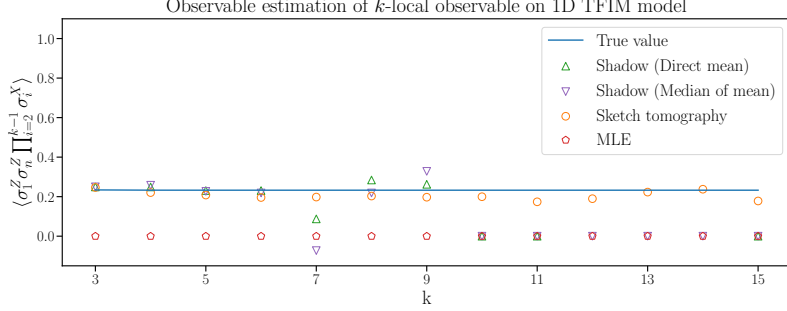


Fig. 5 Predictions of $\langle O_k \rangle = \langle \sigma_1^Z \sigma_n^Z \prod_{i=2}^{k-1} \sigma_i^X \rangle$ for the ground state of the 1D TFIM model. Details on the median-of-mean of classical shadow are in Figure 2. One can see that the prediction from sketch tomography is more accurate than classical shadow and the model trained from the MLE framework.

the mean prediction error is comparable to previous cases at only 0.005. Therefore, $\tilde{\rho}$ is successful in predicting the Renyi entanglement entropy for the majority of the considered subsystems.

4 Conclusion

We present a quantum state tomography method using the classical shadow protocol under the matrix product state assumption. We demonstrate that our approach is highly accurate and sometimes outperforms the classical shadow protocol in observable estimation. Future work can consider extension to other tensor network structures, such as the hierarchical Tucker [13].

Appendix A Literature review

This section provides a comprehensive review of related literature, which consists of the following three parts.

Classical shadow in quantum observable estimation Classical shadow [7] is a protocol that allows experimenters to predict M observables of a quantum state ρ with only $\log(M)$ copies of ρ . The procedure only requires repeated single-copy measurements of ρ . The terminology is inspired by shadow tomography, which Aaronson

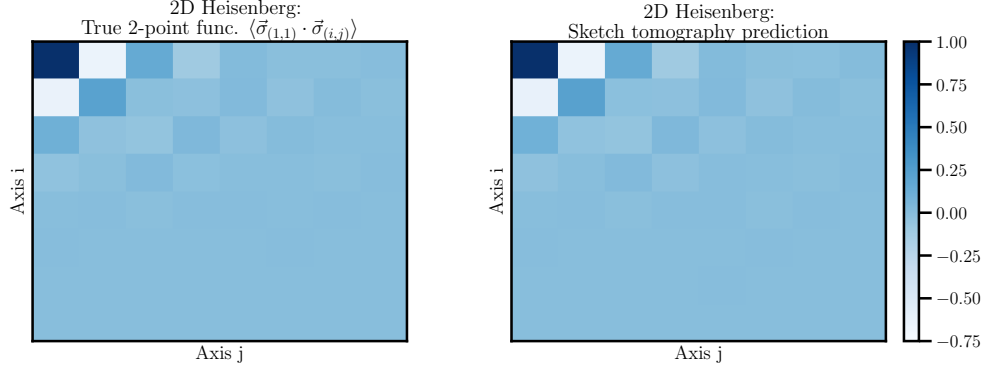


Fig. 6 Predictions of two-point functions $\langle \sigma_{(1,1)} \cdot \sigma_{(i,j)} \rangle$ for the ground state of the 2D Heisenberg model with $n = 64$ lattice sites. One can see that our QST procedure successfully approximates the true 2-point correlation function.

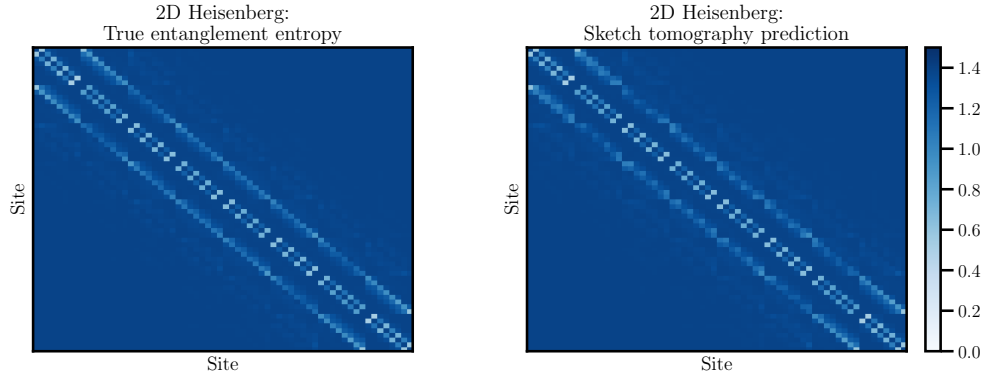


Fig. 7 Prediction of second-order Renyi entanglement entropy for all subsystems of size at most two in the 2D Heisenberg model with $n = 64$ lattice sites. The predicted values using our QST output visually match the true values.

coined in [14]. One can also view the classical shadow estimator as a projected least-squares predictor [15]. Classical shadow has different procedures to perform random uniform scrambling on the state ρ . In [7], the authors propose random Pauli measurement and random Clifford scrambling, the former of which can be implemented with a circuit of depth one, whereas the latter is significantly more involved in terms of circuit complexity. One can also consider other random scrambling protocols of intermediate complexity [16–18]. While our work only considers the random Pauli measurement setting, future work might also consider other random scrambling protocols.

Quantum state tomography Quantum state tomography (QST) is a fundamental task related to learning and engineering high-dimensional quantum systems in many-body physics. Specifically, it aims to reconstruct an unknown quantum state from a collection of experimental measurements. An extensive body of work has explored QST from many different aspects. For instance, one prominent line of work

formulates QST as a matrix recovery problem [15, 19–34], where the density matrix is estimated via statistical techniques such as projected least squares, semidefinite programming, compressed sensing [35–38] and non-convex programming. Moreover, to alleviate the high computational cost of general QST, researchers have adopted simplifying assumptions by considering quantum states that can be well approximated by matrix product states with low bond dimension. This leads to the development of matrix product state tomography [3, 39–47] and variants such as multiscale entangled states tomography [48]. Furthermore, an alternative approach to tackling the high dimensionality of quantum state tomography is to employ machine learning-based methods, such as neural networks [4, 49–58] and generative models [12, 59]. Building upon the aforementioned methodologies and measurement protocols such as classical shadows [7], QST and its variants have inspired numerous related studies and applications, such as theoretical analyses of QST [60–62], quantum measurement tomography [63–68] and quantum process tomography [69–72].

We discuss a few related works that our work bears the most resemblance to. Our work considers performing QST procedures based on the classical shadow approximation, and our work uses a sketching algorithm to reconstruct the true state. In [8, 45], the authors consider a sketching-based procedure for MPS, but they do not use classical shadow, and the procedure does not have a convergence guarantee. In [46, 73, 74], the authors consider a variational approach to train a matrix product operator (MPO) ansatz based on minimizing measurement error, where the proposed algorithm does not have a formal convergence guarantee, and the system size in the experiments remains relatively small. In [75], the authors consider directly fitting an MPO ansatz to fit the classical shadow approximation $\hat{\rho}$, but the procedure uses classical shadow protocol under Haar-random projective measurements, whereas our work focuses on the Pauli measurement setting.

Tensor trains (matrix product states) in quantum physics The tensor train (TT) or matrix product state (MPS) ansatz, which originates from the density matrix renormalization group (DMRG) algorithm [5], provides an efficient parametrization of entangled quantum states in high-dimensional Hilbert spaces. For a complete discussion of TT/MPS and its variants, we refer the readers to the following review articles [76–79]. As one of the most powerful tools in quantum many-body physics, the TT/MPS ansatz and its variants have been applied to a wide range of related tasks. Examples of such tasks include but are not limited to computing ground states via quantum Monte Carlo methods [80–83], studies of electronic structure theory and quantum chemistry [84, 85], simulating open quantum systems and quantum dynamics in general [86–113], solving quantum impurity models [114–133], quantum simulation and quantum computing [134–140], studies of quantum field theories [141–146], representing and learning Feynman diagrams [147, 148], etc.

Appendix B Notations

In addition to the notations of tensors and tensor networks covered above, we provide a brief review of other mathematical notations in this section. We use \otimes to denote the tensor product. For measuring distances between probability distributions,

we use $D_{\text{KL}}(\cdot, \cdot)$ to denote the Kullback-Leibler (KL) divergence between any two probability distributions. For two probability distributions P, Q , we use $P \ll Q$ to mean that P is absolutely continuous with respect to Q . With fixed $d \in \mathbb{N}$, we use \mathbf{I}_d to denote the identity matrix of size $d \times d$. For any complex vector $\mathbf{a} \in \mathbb{C}^d$, we use \mathbf{a}^\top and \mathbf{a}^* to denote the transpose and conjugate transpose of \mathbf{a} , respectively. Moreover, the dot product between any two square matrices $A, B \in \mathbb{C}^{d \times d}$ is denoted by $\langle A, B \rangle_F = \text{tr}[A^* B]$, where A^* denotes the conjugate transpose of A . Regarding the notation of norms, we use $\|\cdot\|_1$ and $\|\cdot\|_F$ to denote the l_1 norm and the Frobenius norm, respectively. In particular, for any vector $v \in \mathbb{C}^n$ and matrix $M \in \mathbb{C}^{m \times n}$, we use $\|v\|$ and $\|M\| = \sup_{\|u\|=1} \|Mu\|$ to denote the l_2 norm of v and the induced operator 2-norm of M , respectively. The singular values of M are denoted by $s_1(M) \geq s_2(M) \geq \dots \geq s_l(M)$, where $l = \min\{m, n\}$. For any $p \in (0, 1)$, the Bernoulli distribution with mean p is denoted by $\text{Ber}(p)$. For any two given quantities f and g , we write $f \gtrsim g$ when the inequality $f \geq Cg$ holds for some fixed constant $C > 0$. Finally, we use the standard symbols X, Y, Z to denote the Pauli matrices in $\mathbb{C}^{2 \times 2}$, which satisfy

$$X = \begin{bmatrix} 0 & 1 \\ 1 & 0 \end{bmatrix}, \quad Y = iXZ = \begin{bmatrix} 0 & -i \\ i & 0 \end{bmatrix}, \quad Z = \begin{bmatrix} 1 & 0 \\ 0 & -1 \end{bmatrix}.$$

Appendix C Details for the sketch tomography procedure

We go through the detailed procedure and derivation for sketch tomography. We assume basic familiarity with the tensor network ansatz and tensor diagrams.

C.1 TT representation of ρ

We first verify the claim in the main text that ρ has a TT format when the target state $|\psi\rangle$ is a matrix product state. In terms of a tensor diagram, one can represent $|\psi\rangle$ as follows:

$$\begin{array}{c} \boxed{|\psi\rangle} \\ \downarrow \downarrow \dots \downarrow \\ j_1 \quad j_2 \quad \dots \quad j_n \end{array} = \begin{array}{c} \boxed{F_1} \text{---} \boxed{F_2} \text{---} \dots \text{---} \boxed{F_n} \\ \downarrow \quad \quad \downarrow \quad \quad \quad \downarrow \\ j_1 \quad \quad j_2 \quad \quad \quad j_n \end{array}. \quad (\text{C1})$$

As is shown in Equation (C1), there exists a collection of n tensor components $(F_k)_{k=1}^n$, where $F_1 \in \mathbb{C}^{2 \times a_1}$, $F_k \in \mathbb{C}^{a_{k-1} \times 2 \times a_k}$ for $k = 2, \dots, n-1$, and $F_n \in \mathbb{C}^{a_{n-1} \times 2}$. The evaluation of any entry in $|\psi\rangle$ is shown in Equation (C1), and one can write it equivalently as follows:

$$|\psi\rangle(j_1, \dots, j_n) = \sum_{\gamma_1, \dots, \gamma_{n-1}} F_1(j_1, \gamma_1) F_2(\gamma_1, j_2, \gamma_2) \dots F_n(\gamma_{n-1}, j_n). \quad (\text{C2})$$

The associated density matrix $\rho = |\psi\rangle\langle\psi|$ is the target object that sketch tomography approximates. One can first use Equation (C1) to directly write ρ in a tensor

diagram as follows:

$$\begin{array}{c} j'_1 \quad j'_2 \quad \dots \quad j'_n \\ \boxed{\rho} \\ j_1 \quad j_2 \quad \dots \quad j_n \end{array} = \begin{array}{c} j'_1 \quad j'_2 \quad \dots \quad j'_n \\ \boxed{\bar{F}_1} \quad \boxed{\bar{F}_2} \quad \dots \quad \boxed{\bar{F}_n} \\ \boxed{F_1} \quad \boxed{F_2} \quad \dots \quad \boxed{F_n} \\ j_1 \quad j_2 \quad \dots \quad j_n \end{array}. \quad (\text{C3})$$

We derive the TT format of ρ by writing Equation (C3) with the Pauli matrices as the basis. For $k \in [n]$, we let $(\sigma_k^X, \sigma_k^Y, \sigma_k^Z)$ denote the Pauli matrices on site k , and we write $(\sigma_k^1, \sigma_k^2, \sigma_k^3, \sigma_k^4) = (\frac{1}{\sqrt{2}}I_2, \frac{1}{\sqrt{2}}\sigma_k^X, \frac{1}{\sqrt{2}}\sigma_k^Y, \frac{1}{\sqrt{2}}\sigma_k^Z)$. The Pauli matrices $(\sigma_k^i)_{i \in [4], k \in [n]}$ allow one to write Equation (C3) in a TT format. We construct tensor components $(G_k)_{k=1}^n$ directly from the MPS ansatz of $|\psi\rangle$ by the following tensor diagrams:

$$\begin{array}{c} i \\ \boxed{G_k} \end{array} = \begin{array}{c} \boxed{\bar{F}_k} \\ \boxed{\sigma_k^i} \\ \boxed{F_k} \end{array}, \quad \begin{array}{c} i \\ \boxed{G_1} \end{array} = \begin{array}{c} \boxed{\bar{F}_1} \\ \boxed{\sigma_1^i} \\ \boxed{F_1} \end{array}, \quad \begin{array}{c} i \\ \boxed{G_n} \end{array} = \begin{array}{c} \boxed{\bar{F}_n} \\ \boxed{\sigma_n^i} \\ \boxed{F_n} \end{array}. \quad (\text{C4})$$

In other words, for $k \notin \{1, n\}$, we construct $G_k \in \mathbb{R}^{a_{k-1}^2 \times 4 \times a_k^2}$ by

$$G_k((\gamma_{k-1}, \gamma'_{k-1}), i, (\gamma_k, \gamma'_k)) = \sum_{j, j'} \sigma_k^i(j, j') F_k(\gamma_{k-1}, j, \gamma_k) \bar{F}_k(\gamma'_{k-1}, j', \gamma'_k), \quad (\text{C5})$$

and the construction for G_1 and G_n can be likewise derived from Equation (C5) by respectively omitting the $(\gamma_{k-1}, \gamma'_{k-1})$ variable and the (γ_k, γ'_k) variable. Lastly, Equation (C5) shows that the entries of G_k are defined by an inner product between two Hermitian matrices, and so all entries of G_k are real numbers.

We now verify that ρ admits a TT format given by $(G_k)_{k=1}^n$. Because multi-linear products of Pauli matrices form a basis in the space of Hermitian matrices in $\mathbb{C}^{2^n \times 2^n}$, there exists a tensor $C: [4]^n \rightarrow \mathbb{R}$ whereby the term ρ is given by

$$\rho = \sum_{i_1, \dots, i_n=1}^4 C(i_1, \dots, i_n) \prod_{l=1}^n \sigma_l^{i_l}.$$

Moreover, the orthonormality of the Pauli matrices implies the following equation

$$C(i_1, \dots, i_n) = \sum_{j_1, j'_1, \dots, j_n, j'_n} \rho((j_1, j'_1), \dots, (j_n, j'_n)) \prod_{l=1}^n \sigma_l^{i_l}(j_l, j'_l).$$

Therefore, one can plug in the definition of ρ in Equation (C3) to directly derive C . One has

$$\begin{array}{c} \boxed{C} \\ \begin{array}{c} i_1 \quad i_2 \quad \dots \quad i_n \end{array} \end{array} = \begin{array}{c} \boxed{\bar{F}_1} \quad \boxed{\bar{F}_2} \quad \dots \quad \boxed{\bar{F}_n} \\ \begin{array}{c} \boxed{\sigma_1^{i_1}} \quad \boxed{\sigma_2^{i_2}} \quad \dots \quad \boxed{\sigma_n^{i_n}} \\ \boxed{F_1} \quad \boxed{F_2} \quad \dots \quad \boxed{F_n} \end{array} \end{array} = \begin{array}{c} \boxed{G_1} \quad \boxed{G_2} \quad \dots \quad \boxed{G_n} \\ \begin{array}{c} i_1 \quad i_2 \quad \dots \quad i_n \end{array} \end{array},$$

where the second equality is from Equation (C4).

C.2 Sketch tomography algorithm for quantum state tomography

We cover how to approximate ρ with the classical shadow protocol. The main idea for the procedure is covered in the main text, and here we go through the full implementation details.

We explain how one applies the classical shadow protocol from Pauli measurements. Let B be the number of recorded measurements. The classical shadow protocol uses the measurement outcome to produce a collection of 2×2 matrices $\{M_l^{(j)} \in \mathbb{C}^{2 \times 2}\}_{l \in [n], j \in [B]}$. The resultant classical shadow approximation $\hat{\rho}$ is written as a sum of separable matrices as follows:

$$\hat{\rho} = \frac{1}{B} \sum_{j=1}^B \bigotimes_{l=1}^n M_l^{(j)}. \quad (\text{C6})$$

Equation (C6) allows for an efficient calculation of the partial trace of $\hat{\rho}$. Therefore, performing observable approximation over Equation (C6) is efficient for any local observable O . When O is k -local, the estimator $\text{tr}[O\hat{\rho}]$ is unbiased with a variance bounded from above by $\mathcal{O}(4^k)$, which is moderate for small k .

In practice, instead of a single classical shadow approximation $\hat{\rho}$ obtained from B experiments on ρ , one can repeat the same protocol W times to form classical shadow approximators $\hat{\rho}_1, \dots, \hat{\rho}_W$. Then, the observable approximation is done by

$$\langle O \rangle = \text{tr}[O\rho] \approx \text{median}\{\text{tr}[O\hat{\rho}_1], \dots, \text{tr}[O\hat{\rho}_W]\},$$

where $\text{median}\{a_1, \dots, a_W\}$ is the median of the W scalars a_1, \dots, a_W . The median-of-mean estimator is unbiased and is more robust with respect to outliers.

We go through our QST procedure for obtaining ρ . For notational compactness, for an index set $S = \{s_1, \dots, s_l\} \subset [d]$, we use a multi-index notation by letting $i_S := (i_{s_1}, \dots, i_{s_l})$, i.e. i_S stands for the subvector of variables with entries from the index set S . Using the multi-index notation, any density matrix ρ can be uniquely

represented by a tensor $C: [4]^n \rightarrow \mathbb{R}$ as follows:

$$\rho = \sum_{i_{[n]} \in [4]^n} C(i_{[n]}) \prod_{l=1}^n \sigma_l^{i_l}.$$

Given the MPS assumption on $|\psi\rangle$, the tensor C can be written in terms of tensor components $(G_k)_{k=1}^n$, where $G_1 \in \mathbb{R}^{4 \times r_1}$, $G_k \in \mathbb{R}^{r_{k-1} \times 4 \times r_k}$ for $k = 2, \dots, n-1$, and $G_n \in \mathbb{R}^{r_{n-1} \times 4}$. The equation for C is written as follows:

$$C(i_{[n]}) = \sum_{\alpha_{[n-1]}} G_1(i_1, \alpha_1) G_2(\alpha_1, i_2, \alpha_2) \cdots G_n(\alpha_{n-1}, i_n). \quad (\text{C7})$$

To obtain ρ , we obtain each G_k for $k = 1, \dots, n$. We first cover the case where $k \notin \{1, n\}$. Due to the structural equation in Equation (C7), there exist tensors $C_{<k}: [4]^{k-1} \times [r_{k-1}] \rightarrow \mathbb{R}$ and $C_{>k}: [r_k] \times [4]^{n-k} \rightarrow \mathbb{R}$ so that the following equation holds:

$$\sum_{\alpha_{k-1}, \alpha_k} C_{<k}(i_{[k-1]}, \alpha_{k-1}) G_k(\alpha_{k-1}, i_k, \alpha_k) C_{>k}(\alpha_k, i_{[n]-[k]}) = C(i_{[n]}). \quad (\text{C8})$$

One then applies sketching to Equation (C8) to form a tractable linear system for G_k . We let $\tilde{r}_{k-1}, \tilde{r}_k$ be two integers such that $\tilde{r}_{k-1} \geq r_{k-1}$ and $\tilde{r}_k \geq r_k$. We introduce two sketch tensors $S_{<k}: [\tilde{r}_{k-1}] \times [4]^{k-1} \rightarrow \mathbb{R}$, $S_{>k}: [4]^{n-k} \times [\tilde{r}_k] \rightarrow \mathbb{R}$. By contracting Equation (C8) with $S_{>k}$ and $S_{<k}$, one obtains

$$\sum_{\alpha_{k-1}, \alpha_k} A_{<k}(\zeta, \alpha_{k-1}) G_k(\alpha_{k-1}, i_k, \alpha_k) A_{>k}(\alpha_k, \mu) = B_k(\zeta, i_k, \mu), \quad (\text{C9})$$

where $A_{>k}, A_{<k}$ are respectively the contraction of $C_{>k}, C_{<k}$ by $S_{>k}, S_{<k}$ over $i_{[n]-[k]}, i_{[k-1]}$ and B_k is the contraction of C by $S_{>k} \otimes S_{<k}$ over $i_{[n]-\{k\}}$.

In practice, the contractions are done *implicitly* through taking observables. We let $\{L_k^\zeta\}_{\zeta \in [\tilde{r}_{k-1}]}$ and $\{R_k^\mu\}_{\mu \in [\tilde{r}_k]}$ be observables associated with $S_{<k}, S_{>k}$ through the following equation:

$$L_k^\zeta = \sum_{i_{[k-1]}} S_{<k}(\zeta, i_{[k-1]}) \prod_{l=1}^{k-1} \sigma_l^{i_l}, \quad R_k^\mu = \sum_{i_{[n]-[k]}} S_{>k}(i_{[n]-[k]}, \mu) \prod_{l=k+1}^n \sigma_l^{i_l}. \quad (\text{C10})$$

Then, to calculate B_k , we utilize the fact that $\{\prod_{l=1}^n \sigma_l^{i_l}\}_{i_{[n]} \in [4]^n}$ is an orthonormal basis in the space of Hermitian matrices in $\mathbb{C}^{2^n \times 2^n}$, and so the following holds for B_k :

$$B_k(\zeta, i_k, \mu) = \sum_{i_{[n]-\{k\}}} C(i_{[n]}) S_{<k}(\zeta, i_{[k-1]}) S_{>k}(i_{[n]-[k]}, \mu) = \text{tr} \left[\rho L_k^\zeta \sigma_k^{i_k} R_k^\mu \right],$$

where the second equality holds by the definition of $\{L_k^\zeta\}_{\zeta \in [\tilde{r}_{k-1}]}$ and $\{R_k^\mu\}_{\mu \in [\tilde{r}_k]}$. With the classical shadow protocol, we approximate B_k by

$$B_k(\zeta, i_k, \mu) \approx \text{median} \left\{ \text{tr} \left[\hat{\rho}_1 L_k^\zeta \sigma_k^{i_k} R_k^\mu \right], \dots, \text{tr} \left[\hat{\rho}_W L_k^\zeta \sigma_k^{i_k} R_k^\mu \right] \right\}. \quad (\text{C11})$$

There exists a gauge degree of freedom for the TT representation of C at each internal bond of the tensor. More explicitly, the pair of tensors $(C_{>k}, C_{<(k+1)})$ determines the value of $(A_{>k}, A_{<(k+1)})$, and so obtaining $A_{>k}$ is dependent on fixing the gauge on $(C_{>k}, C_{<(k+1)})$. To fix the gauge and obtain $A_{<k}, A_{>k}$, we assume that all sketch tensors $\{S_{>1}\} \cup \{S_{>j}, S_{<j}\}_{j=2}^{n-1} \cup \{S_{<n}\}$ have been defined via Equation (C10). We use sketching of C to uniquely determine a gauge on $(C_{>k}, C_{<(k+1)})$.

To obtain $A_{>k}$, we construct a tensor Z_k from contracting C with $S_{<(k+1)} \otimes S_{>k}$. By associating $S_{<(k+1)}$ with observables $\{L_{k+1}^{\zeta'}\}_{\zeta' \in [\tilde{r}_k]}$, we have

$$Z_k(\zeta', \mu) = \text{tr} \left[\rho L_{k+1}^{\zeta'} R_k^\mu \right] \approx \text{median} \left\{ \text{tr} \left[\hat{\rho}_1 L_{k+1}^{\zeta'} R_k^\mu \right], \dots, \text{tr} \left[\hat{\rho}_W L_{k+1}^{\zeta'} R_k^\mu \right] \right\}, \quad (\text{C12})$$

where the equality holds by the definition of $\{L_{k+1}^{\zeta'}\}_{\zeta' \in [\tilde{r}_k]}$ and $\{R_k^\mu\}_{\mu \in [\tilde{r}_k]}$. The SVD of Z_k uniquely determines the best rank- r_k factorization $Z_k = U S V^\top$. For example, the choice of setting $A_{<(k+1)} = U$ and $A_{>k} = S V^\top$ uniquely fixes the gauge of $(C_{>k}, C_{<(k+1)})$. One way to understand the construction is that $C_{>k}$ is chosen to be the unique tensor for which the contraction of $C_{>k}$ with $S_{>k}$ is U . Finally, obtaining $A_{<k}$ is done through the best rank- r_{k-1} factorization of Z_{k-1} .

We now detail the procedure for $k = 1$ and $k = n$. For G_1 and G_n , one can likewise use sketch tensors $S_{>1}$ and $S_{<n}$ to form the following linear system

$$\begin{aligned} \sum_{\alpha_1} G_1(i_1, \alpha_1) A_{>1}(\alpha_1, \mu) &= B_1(i_1, \mu), \\ \sum_{\alpha_{n-1}} A_{<n}(\zeta, \alpha_{n-1}) G_n(\alpha_{n-1}, i_n) &= B_n(\zeta, i_n). \end{aligned} \quad (\text{C13})$$

The term $A_{>1}$ and $A_{<n}$ are respectively obtained using Z_1 and Z_{n-1} obtained via Equation (C12). Lastly, the sketch tensors $S_{>1}, S_{<n}$ are respectively defined implicitly with observables $\{R_1^\mu\}_{\mu \in [\tilde{r}_1]}$ and $\{L_n^\zeta\}_{\zeta \in [\tilde{r}_{n-1}]}$. One obtains B_1 and B_n by

$$\begin{aligned} B_1(i_1, \mu) &\approx \text{median} \left\{ \text{tr} \left[\hat{\rho}_1 \sigma_1^{i_1} R_1^\mu \right], \dots, \text{tr} \left[\hat{\rho}_W \sigma_1^{i_1} R_1^\mu \right] \right\}, \\ B_n(\zeta, i_n) &\approx \text{median} \left\{ \text{tr} \left[\hat{\rho}_1 L_n^\zeta \sigma_n^{i_n} \right], \dots, \text{tr} \left[\hat{\rho}_W L_n^\zeta \sigma_n^{i_n} \right] \right\}. \end{aligned} \quad (\text{C14})$$

We summarize our approach in Algorithm 1. We use the classical shadow to obtain each Z_k, B_k and we use SVD on each Z_k to obtain all $A_{>k}, A_{<k}$. Then, solving the corresponding sketched linear equation for all G_k allows one to obtain a TT approximation of ρ .

Algorithm 1 Sketch tomography for quantum state tomography under MPS assumption

Require: Classical shadow approximation $\{\hat{\rho}_1, \dots, \hat{\rho}_W\}$ from Equation (C6).

Require: Collection of sketch tensors $\{S_{>k}, S_{<k}\}$

Require: Target internal ranks $\{r_k\}$ for $k = 1, \dots, n-1$.

```

1: for  $k = 1, \dots, n-1$  do
2:   Obtain  $Z_k$  by Equation (C12).
3:   Obtain  $A_{<(k+1)}$  and  $A_{>k}$  respectively as the left and right factor of the best
      rank- $r_k$  factorization of  $Z_k$ .
4: end for
5: for  $k = 1, \dots, n$  do
6:   if  $k = 1$  or  $k = n$  then
7:     Obtain  $B_k$  by Equation (C14).
8:     Obtain  $\hat{G}_k \approx G_k$  by solving the linear system in Equation (C13).
9:   end if
10:  if  $k \notin \{1, n\}$  then
11:    Obtain  $B_k$  by Equation (C11).
12:    Obtain  $\hat{G}_k \approx G_k$  by solving the linear system in Equation (C9).
13:  end if
14: end for
15: Output the approximate density matrix  $\tilde{\rho}$  with tensor component  $(\hat{G}_k)_{k=1}^n$ .

```

Appendix D Proof of the upper bound

This section goes through the convergence guarantee for the sketch tomography procedure. The ground truth is a density matrix ρ whose coefficient tensor is a tensor train. Sketch tomography takes in the classical shadow approximation $\hat{\rho}$ and outputs an approximate density matrix $\tilde{\rho}$ with tensor component $(\hat{G}_k)_{k=1}^n$. The organization of this section is as follows. In Section D.1, we state the necessary assumptions for the results of this section. In Section D.2, we show that each observable estimation task required by Algorithm 1 is accurate. In Section D.3, we prove that each tensor component of $\tilde{\rho}$ is close to the tensor component of ρ . In Section D.4, we prove that $\tilde{\rho}$ is close to ρ in the Frobenius norm.

Notations We summarize the necessary notations for the analysis. For a vector v , the term $\|v\|$ is its l_2 norm. For a matrix M , the term $\|M\|$ is its operator norm, and the term $s_j(M)$ is the j -th singular value of M . For a tensor G , the term $\|G\|_F$ is the Frobenius norm of G . We also assume the multi-index notation used in Appendix C.

D.1 Assumptions

We list out the assumptions for the convergence guarantee of sketch tomography. As in Appendix C, we use ρ to represent the target density matrix on n qubits. For easy reference, we summarize the construction of the Pauli-basis representation of ρ :

Definition 1 We let $(\sigma_k^X, \sigma_k^Y, \sigma_k^Z)$ denote the Pauli matrices on site $k \in [n]$, and we write $(\sigma_k^1, \sigma_k^2, \sigma_k^3, \sigma_k^4) = (\frac{1}{\sqrt{2}}I_2, \frac{1}{\sqrt{2}}\sigma_k^X, \frac{1}{\sqrt{2}}\sigma_k^Y, \frac{1}{\sqrt{2}}\sigma_k^Z)$. The density matrix ρ admits a *coefficient tensor* C which characterizes ρ by the following equation:

$$\rho = \sum_{i_{[n]} \in [4]^n} C(i_{[n]}) \prod_{l=1}^n \sigma_l^{i_l}. \quad (\text{D15})$$

In particular, each entry of C is constructed from ρ as follows:

$$C(i_1, \dots, i_n) = \text{tr} \left[\rho \prod_{l=1}^n \sigma_l^{i_l} \right]. \quad (\text{D16})$$

Following Definition 1, we formalize the tensor train (TT) property on ρ as an assumption. In particular, Appendix C shows that the following TT assumption on ρ holds when ρ is the density matrix of a matrix product state $|\psi\rangle$.

Assumption 1 The coefficient tensor C defined from Definition 1 is a tensor train. In particular, there exists a collection of internal rank $\{r_k\}_{k=1}^{n-1}$ and a collection of tensor components $(G_k)_{k=1}^n$, where $G_1 \in \mathbb{R}^{4 \times r_1}$, $G_k \in \mathbb{R}^{r_{k-1} \times 4 \times r_k}$ for $k = 2, \dots, n-1$, and $G_n \in \mathbb{R}^{r_{n-1} \times 4}$. The tensor C is defined by $(G_k)_{k=1}^n$ by the following equation:

$$C(i_{[n]}) = \sum_{\alpha_{[n-1]}} G_1(i_1, \alpha_1) G_2(\alpha_1, i_2, \alpha_2) \cdots G_n(\alpha_{n-1}, i_n). \quad (\text{D17})$$

Secondly, we place assumptions to constrain the design space for sketch tensors. As shown in Appendix C, the sketch tensors are defined implicitly through observables. The integers $\{\tilde{r}_k\}_{k=1}^{n-1}$ represent the number of sketch functions used during sketch tomography. The sketching procedure uses sketch tensors $\{S_{<k}, S_{>k}\}_{k=1}^n$ which are defined implicitly through observables. We summarize the construction here:

Definition 2 For $k = 2, \dots, n$, the sketch tensor $S_{<k}$ is associated with observables $\{L_k^\zeta\}_{\zeta \in [\tilde{r}_{k-1}]}$. Each observable L_k^ζ only involves sites to the left of k , i.e. the set $\{1, \dots, k-1\}$. The tensor $S_{<k}$ is defined from $\{L_k^\zeta\}_\zeta$ by the following equation:

$$S_{<k}(\zeta, i_1, \dots, i_{k-1}) = \text{tr} \left[L_k^\zeta \prod_{l=1}^{k-1} \sigma_l^{i_l} \right]. \quad (\text{D18})$$

Similarly, for $k = 1, \dots, n-1$, the sketch tensor $S_{>k}$ is associated with observables $\{R_k^\mu\}_{\mu \in [\tilde{r}_k]}$. Each observable R_k^μ only involves sites to the right of site k , i.e. the set $\{k+1, \dots, n\}$. The tensor $S_{>k}$ is defined from $\{R_k^\mu\}_\mu$ by the following equation:

$$S_{>k}(i_{k+1}, \dots, i_n, \mu) = \text{tr} \left[R_k^\mu \prod_{l=k+1}^n \sigma_l^{i_l} \right]. \quad (\text{D19})$$

The second assumption requires that the associated observables of the sketch tensors should come from local observables. Essentially, this assumption is to ensure that the classical shadow protocol under random Pauli measurement can reliably perform observable estimations required by Algorithm 1.

Assumption 2 For $k = 1, \dots, n-1$, we let $\tilde{r}_k = r_k$, where r_k is the true internal rank in Definition 1. Moreover, each of the observables $\{L_k^\zeta\}_\zeta$ and $\{R_k^\mu\}_\mu$ in Definition 2 is a linear combination of local observables. Essentially, for $M = R_k^\mu$ or $M = L_k^\zeta$, we require that one can write

$$M = \sum_{l=1}^P O_l,$$

where each O_l only involves $\mathcal{O}(1)$ sites. Moreover, we require $\sum_{l=1}^P \|O_l\| = \mathcal{O}(1)$, where $\|\cdot\|$ is the operator norm.

Assumption 2 is a mild assumption on the design of sketch tensors. One way to satisfy Assumption 2 is to set $\{L_k^\zeta\}_\zeta$ and $\{R_k^\mu\}_\mu$ to be a linear combination of 1-local and 2-local Pauli observables with bounded total weights. When running Algorithm 1 with sketch tensors satisfying Assumption 2, one can ensure that all observable estimation done by $\hat{\rho}$ can achieve a high accuracy with a sufficient number of state copies.

The third assumption chooses how one obtains $A_{<(k+1)}$ and $A_{>k}$ from Z_k . While this assumption could be precluded, its inclusion significantly simplifies the error analysis. We state it here:

Assumption 3 From Assumption 2, one has $r_k = \tilde{r}_k$ for $k = 1, \dots, n-1$. Let $Z_k \in \mathbb{R}^{r_k \times r_k}$ be from Equation (C12), we set $A_{<(k+1)}$ and $A_{>k}$ to be a rank- r_k factorization so that

$$A_{<(k+1)} = I_{r_k}, \quad A_{>k} = Z_k.$$

Let \hat{Z}_k be the finite-sample estimation of Z_k . We set $\hat{A}_{<(k+1)}$ and $\hat{A}_{>k}$ to be

$$\hat{A}_{<(k+1)} = I_{r_k}, \quad \hat{A}_{>k} = \hat{Z}_k.$$

This particular gauge choice is made only for the sake of analysis. In practice, one may instead take $(A_{<(k+1)}, A_{>k})$ from the SVD of Z_k ; this corresponds to an orthogonal change of basis on the internal legs and does not affect the asymptotic scaling of our bounds. However, using SVD complicates the notation for error analysis.

D.2 Error bound on observable estimation

Assumption 1 and Assumption 2 allow us to provide an error bound on all of the observable estimation tasks that are performed when running Algorithm 1. To obtain G_k , we have seen in Section 2 that one needs to form three sketches $B_k \in \mathbb{R}^{\tilde{r}_{k-1} \times 4 \times \tilde{r}_k}$, $Z_{k-1} \in \mathbb{R}^{\tilde{r}_{k-1} \times \tilde{r}_{k-1}}$, $Z_k \in \mathbb{R}^{\tilde{r}_k \times \tilde{r}_k}$ by performing observable estimation on ρ . This section bounds the error rate on the sketch estimation.

For the error estimation, we assume that the reader is familiar with the definition of the shadow norm $\|\cdot\|_{\text{shadow}}$ in [7]. For readers unfamiliar with the concept, one can still follow the derivation by assuming the results on $\|\cdot\|_{\text{shadow}}$ from [7]. For a brief explanation, the shadow norm essentially measures the complexity of the observable in a given classical shadow protocol. For random Pauli measurement, estimating $\text{tr}[\rho O]$ is only accurate when $\|O\|_{\text{shadow}}$ is small. Moreover, $\|O\|_{\text{shadow}}$ can be reliably bounded from above when O is a local observable or a sum of local observables. Therefore,

Assumption 2 essentially forces the sketch tensors to correspond to observables that have a small shadow norm.

From the formula in Definition 2, the sketches B_k, Z_{k-1}, Z_k satisfy the following equations:

$$\begin{aligned} B_k(\zeta, i_k, \mu) &= \text{tr} \left[\rho L_k^\zeta \sigma_k^{i_k} R_k^\mu \right], \\ Z_{k-1}(\zeta, \mu') &= \text{tr} \left[\rho L_k^\zeta R_{k-1}^{\mu'} \right], \\ Z_k(\zeta', \mu) &= \text{tr} \left[\rho L_{k+1}^{\zeta'} R_k^\mu \right]. \end{aligned} \tag{D20}$$

During the procedure of Algorithm 1, we use W copies of the classical shadow estimator to form the approximated sketches $\hat{B}_k, \hat{Z}_{k-1}, \hat{Z}_k$ with the following formula:

$$\begin{aligned} \hat{B}_k(\zeta, i_k, \mu) &= \text{median} \left\{ \text{tr} \left[\hat{\rho}_1 L_k^\zeta \sigma_k^{i_k} R_k^\mu \right], \dots, \text{tr} \left[\hat{\rho}_W L_k^\zeta \sigma_k^{i_k} R_k^\mu \right] \right\}, \\ \hat{Z}_{k-1}(\zeta, \mu') &= \text{median} \left\{ \text{tr} \left[\hat{\rho}_1 L_k^\zeta R_{k-1}^{\mu'} \right], \dots, \text{tr} \left[\hat{\rho}_W L_k^\zeta R_{k-1}^{\mu'} \right] \right\}, \\ \hat{Z}_k(\zeta', \mu) &= \text{median} \left\{ \text{tr} \left[\hat{\rho}_1 L_{k+1}^{\zeta'} R_k^\mu \right], \dots, \text{tr} \left[\hat{\rho}_W L_{k+1}^{\zeta'} R_k^\mu \right] \right\}. \end{aligned} \tag{D21}$$

Assumption 2 allows us to bound the error in approximating the formed sketches. We show that one has the following result:

Proposition 3 *Let $\delta, \varepsilon \in (0, 1)$ be accuracy parameters. Let $\tilde{r}_{\max} = \max_{k \in [n-1]} \tilde{r}_k$. In Algorithm 1, set $W = 2 \log(12n\tilde{r}_{\max}^2/\delta)$ and suppose each $\hat{\rho}_w$ with $w \in [W]$ is a classical shadow approximator formed from B measurements. Moreover, suppose $\{S_{<k}, S_{>k}\}_{k=1}^n$ are sketch tensors satisfying Assumption 2. Then, there exists a problem-independent constant c_S such that $B \geq \frac{c_S}{\varepsilon^2}$ ensures that the following events jointly hold with probability $1 - \delta$:*

1. For any $k = 1, \dots, n-1$ and $\zeta, \mu \in [\tilde{r}_k]$,

$$|Z_k(\zeta, \mu) - \hat{Z}_k(\zeta, \mu)| \leq \varepsilon.$$

2. For any $k = 1, \dots, n$ and $\zeta \in [\tilde{r}_{k-1}], i_k \in [4], \mu \in [\tilde{r}_k]$,

$$|B_k(\zeta, i_k, \mu) - \hat{B}_k(\zeta, i_k, \mu)| \leq \varepsilon.$$

Proof The proof requires the reader to be familiar with the shadow norm $\|\cdot\|_{\text{shadow}}$ in [7]. The result is essentially a direct corollary of Assumption 2 and Theorem 1 in [7]. Moreover, while the statement sets c_S to be a problem-independent constant, we provide the value of c_S by specifying the $\mathcal{O}(1)$ constant in Assumption 2.

We consider an observable $L_{k+1}^\zeta R_k^\mu$ corresponding to the term $Z_k(\zeta, \mu)$. By Assumption 2, one can write

$$L_{k+1}^\zeta = \sum_{l=1}^P O_l, \quad R_k^\mu = \sum_{l'=1}^{P'} U_{l'},$$

where each $O_l, U_{l'}$ only involves at most D_1 sites. Moreover, we suppose D_2 is a constant so that

$$\sum_{l=1}^P \|O_l\| \leq D_2, \quad \sum_{l'=1}^{P'} \|U_{l'}\| \leq D_2.$$

By Definition 2, one can see that each O_l only involves site $\{1, \dots, k\}$, and each $U_{l'}$ only involves site $\{k+1, \dots, n\}$. Thus, the observable $L_{k+1}^\zeta R_k^\mu$ can be written as

$$L_{k+1}^\zeta R_k^\mu = \sum_{l=1}^P \sum_{l'=1}^{P'} O_l U_{l'}.$$

For each index (l, l') , one can see that the term $O_l U_{l'}$ only involves $2D_1$ sites. Moreover, as $O_l, U_{l'}$ acts on non-overlapping sites, one has $\|O_l U_{l'}\| = \|O_l\| \|U_{l'}\|$. Therefore, one has

$$\sum_{l=1}^P \sum_{l'=1}^{P'} \|O_l U_{l'}\| = \sum_{l=1}^P \sum_{l'=1}^{P'} \|O_l\| \|U_{l'}\| = \left(\sum_{l=1}^P \|O_l\| \right) \left(\sum_{l'=1}^{P'} \|U_{l'}\| \right) \leq D_2^2.$$

By Proposition 3 in [7], as each term $O_l U_{l'}$ involves only $2D_1$ sites, one has

$$\|O_l U_{l'}\|_{\text{shadow}} \leq 2^{2D_1} \|O_l U_{l'}\|.$$

As [7] has shown that the shadow norm satisfies the triangle inequality, one has

$$\|L_{k+1}^\zeta R_k^\mu\|_{\text{shadow}} \leq \sum_{l=1}^P \sum_{l'=1}^{P'} \|O_l U_{l'}\|_{\text{shadow}} \leq \sum_{l=1}^P \sum_{l'=1}^{P'} 2^{2D_1} \|O_l U_{l'}\| \leq 4^{D_1} D_2^2. \quad (\text{D22})$$

We similarly bound the shadow norm for the observable $L_k^\zeta \sigma_k^{i_k} R_k^\mu$ corresponding to the term $B_k(\zeta, i_k, \mu)$. Again, using Assumption 2, one can write

$$L_k^\zeta = \sum_{l=1}^{\tilde{P}} \tilde{O}_l,$$

so that \tilde{O}_l only acts on D_1 sites and $\sum_{l=1}^{\tilde{P}} \|\tilde{O}_l\| \leq D_2$. Then, one has

$$L_k^\zeta \sigma_k^{i_k} R_k^\mu = \sum_{l=1}^{\tilde{P}} \sum_{l'=1}^{P'} \tilde{O}_l \sigma_k^{i_k} U_{l'}.$$

We can see that $O_l \sigma_k^{i_k} U_{l'}$ acts on $2D_1 + 1$ sites, and so Proposition 3 in [7] similarly shows

$$\|\tilde{O}_l \sigma_k^{i_k} U_{l'}\|_{\text{shadow}} \leq 2^{2D_1+1} \|\tilde{O}_l \sigma_k^{i_k} U_{l'}\| = 2^{2D_1+1/2} \|\tilde{O}_l\| \|U_{l'}\|,$$

where the last equality uses the separability of the observable and the fact that $\|\sigma_k^i\| = \frac{1}{\sqrt{2}}$ for $i \in [4]$. Then, by the triangle inequality on $\|\cdot\|_{\text{shadow}}$, one has

$$\|L_k^\zeta \sigma_k^{i_k} R_k^\mu\|_{\text{shadow}} \leq \sum_{l=1}^{\tilde{P}} \sum_{l'=1}^{P'} \|\tilde{O}_l \sigma_k^{i_k} U_{l'}\|_{\text{shadow}} \leq \sum_{l=1}^{\tilde{P}} \sum_{l'=1}^{P'} 2^{2D_1+1/2} \|\tilde{O}_l\| \|U_{l'}\| \leq 4^{D_1+1/4} D_2^2. \quad (\text{D23})$$

Therefore, when running Algorithm 1, we require the classical shadow protocol to perform M observable estimation tasks on observable Q_1, \dots, Q_M . In this case, one has $M \leq 6n\tilde{r}_{\max}^2$ and $\|Q_i\|_{\text{shadow}} \leq 4^{D_1+1/4} D_2^2$. We can now use Theorem 1 in [7], and one can see that taking $c_S = 68 \times 16^{D_1} D_2^4$ is sufficient for Theorem 3 to hold. \square

For the constant c_S , one typically takes $D_1 = 2$ and $D_2 = 1$ to ensure the classical shadow procedure is successful. In practice, instead of enforcing Assumption 2, one can also directly design sketch tensors so that they correspond to observables with a small shadow norm.

D.3 Error bound on tensor component G_k

This section proves the component-wise convergence result. Algorithm 1 outputs a series of tensor components $(\hat{G}_k)_{k=1}^n$ to form an approximation $\tilde{\rho}$. We prove that the output \hat{G}_k accurately approximates G_k .

Proposition 4 (Local error bound on sketch tomography) *Let $\rho \in \mathbb{C}^{2^n \times 2^n}$ be a density matrix satisfying Assumption 1. Moreover, let $\{S_{<k}, S_{>k}\}_{k=1}^n$ be sketch tensors satisfying Assumption 2, and let Algorithm 1 satisfy Assumption 3. Let the true sketch $\{B_k\}_{k=1}^n$ and $\{Z_k\}_{k=1}^{n-1}$ be as in Equation (D20). Moreover, let the approximated sketch $\{\hat{B}_k\}_{k=1}^n$ and $\{\hat{Z}_k\}_{k=1}^{n-1}$ be as in Equation (D21), and let $\{\hat{G}_k\}_{k=1}^n$ be the obtained tensor component from Algorithm 1.*

Let $\varepsilon_1, \varepsilon_2$ be two accuracy parameters so that the classical shadow estimate satisfies

$$\max_{k \in [n-1]} \|Z_k - \hat{Z}_k\| \leq \varepsilon_1, \quad \max_{k \in [n]} \|B_k - \hat{B}_k\|_F \leq \varepsilon_2.$$

Moreover, suppose that $\varepsilon_1 \leq \frac{1}{2} \min_{k \in [n-1]} s_{r_k}(Z_k)$. Then, for $k = 1, \dots, n$, one has

$$\|\hat{G}_k - G_k\|_F^2 \leq 2c_Z^2(c_G^2\varepsilon_1^2 + \varepsilon_2^2), \quad (\text{D24})$$

where the constant c_Z is given by $c_Z = \max\left(1, \max_{k \in [n-1]} \frac{2}{s_{r_k}(Z_k)}\right)$, and c_G is given by $c_G = \max(1, \max_{k \in [n]} \|G_k\|_F)$.

In particular, let $\varepsilon \in (0, 1)$ be an accuracy parameter and let c_S, r_{\max} be the same term as in Theorem 3. In Algorithm 1, set $W = 2 \log(12n\tilde{r}_{\max}^2/\delta)$ and set $B \geq 2c_S r_{\max}^2 c_Z^2 (c_G^2 + 4)\varepsilon^{-2}$. Then, with probability $1 - \delta$, the following holds for all $k = 1, \dots, n$:

$$\|\hat{G}_k - G_k\|_F \leq \varepsilon. \quad (\text{D25})$$

For the error analysis, we need to invoke a result on the stability of the least-squares solution under perturbations of the linear system.

Lemma 1 (Corollary to Theorem 3.48 of [149]) *Let $A \in \mathbb{R}^{m \times r}$ be of rank r . Let ΔA be a perturbation with $\|A^\dagger\| \|\Delta A\| \leq \frac{1}{2}$. Let $b, \Delta b \in \mathbb{R}^m$. Let v satisfy $Av = b$, and let \hat{v} be the least-squares solution to $(A + \Delta A)x = b + \Delta b$. Then one has*

$$\|\hat{v} - v\| \leq 2\|A^\dagger\| (\|\Delta A\| \|v\| + \|\Delta b\|).$$

We now present the proof of Theorem 4.

Proof We first prove Equation (D24), and we then show that Equation (D25) holds as a consequence. The main idea for the proof lies in the error analysis on the sketched linear equation for G_k and \hat{G}_k . We first consider the case where k is not a boundary node. By Assumption 3, the linear equation for G_k reads as follows:

$$\sum_{\alpha_k} G_k(\alpha_{k-1}, i_k, \alpha_k) Z_k(\alpha_k, \mu) = B_k(\alpha_{k-1}, i_k, \mu). \quad (\text{D26})$$

Likewise, obtaining \hat{G}_k is done by solving a perturbed linear system via least-squares. From \hat{Z}_k as in Equation (D21), the linear equation for \hat{G}_k reads:

$$\sum_{\alpha_k} \hat{G}_k(\alpha_{k-1}, i_k, \alpha_k) \hat{Z}_k(\alpha_k, \mu) = \hat{B}_k(\alpha_{k-1}, i_k, \mu). \quad (\text{D27})$$

For any $\alpha_{k-1} \in [r_{k-1}]$, $i_k \in [4]$, we take b, \hat{b} to be the slice of B_k and \hat{B}_k where we take the first index to be α_{k-1} and second index to be i_k . In MATLAB notation, one might write $b = B_k(\alpha_{k-1}, i_k, :)$, $\hat{b} = \hat{B}_k(\alpha_{k-1}, i_k, :)$. Likewise, we take v, \hat{v} to be the slice of G_k and \hat{G}_k where we take the first index to be α_{k-1} and second index to be i_k . Then, one can see that v is the exact solution to $Z_k^\top x = b$, whereas \hat{v} is the least-squares solution to $\hat{Z}_k^\top x = \hat{b}$. Thus, by invoking Lemma 1, one has

$$\|\hat{v} - v\| \leq 2\|A^\dagger\|(\|\Delta A\|\|v\| + \|\Delta b\|) \leq \frac{2}{s_{r_k}(Z_k)}(\varepsilon_1\|v\| + \|\Delta b\|).$$

By the Cauchy-Schwarz inequality, one has

$$\|\hat{v} - v\|^2 \leq 2\left(\frac{2}{s_{r_k}(Z_k)}\right)^2(\varepsilon_1^2\|v\|^2 + \|\Delta b\|^2). \quad (\text{D28})$$

Thus, summing over all (α_{k-1}, i_k) indices, one has

$$\|G_k - \hat{G}_k\|_F^2 \leq 2\left(\frac{2}{s_{r_k}(Z_k)}\right)^2(\varepsilon_1^2\|G_k\|_F^2 + \|\Delta B_k\|_F^2) \leq 2\left(\frac{2}{s_{r_k}(Z_k)}\right)^2(\varepsilon_1^2\|G_k\|_F^2 + \varepsilon_2^2).$$

For $k = n$, one can see that $G_k = B_k$ and $\hat{G}_k = \hat{B}_k$, and so $\|G_k - \hat{G}_k\|_F^2 \leq \varepsilon_2^2$. For $k = 1$, one can repeat the same calculation as in the $1 < k < n$ case. One has

$$\sum_{\alpha_1} G_1(i_1, \alpha_1) Z_1(\alpha_1, \mu) = B_1(i_1, \mu), \quad \sum_{\alpha_1} \hat{G}_1(i_1, \alpha_1) \hat{Z}_1(\alpha_1, \mu) = \hat{B}_1(i_1, \mu). \quad (\text{D29})$$

For any $i_1 \in [4]$, one can take b, \hat{b} to be the slice of B_1 and \hat{B}_1 where we take the first index to be i_1 , and one takes v, \hat{v} to be the slice of G_1 and \hat{G}_1 where we take the first index to be i_1 . By invoking Lemma 1 and repeating the exact same calculation for $1 < k < n$, one obtains $\|G_1 - \hat{G}_1\|_F^2 \leq 2\left(\frac{2}{s_{r_1}(Z_1)}\right)^2(\varepsilon_1^2\|G_1\|_F^2 + \varepsilon_2^2)$. We have thus shown that Equation (D24) holds for all $k \in [n]$.

We now show that Equation (D25) holds with high probability. First, we let $\tilde{\varepsilon} > 0$ be a parameter to be specified. We employ Theorem 3. For $B \geq c_S \tilde{\varepsilon}^{-2}$, simple norm equivalence shows that the following two bounds jointly hold with probability $1 - \delta$:

$$\max_{k \in [n-1]} \|Z_k - \hat{Z}_k\| \leq r_{\max} \tilde{\varepsilon}, \quad \max_{k \in [n]} \|B_k - \hat{B}_k\|_F \leq 2r_{\max} \tilde{\varepsilon}.$$

Suppose that $r_{\max} \tilde{\varepsilon} \leq \frac{1}{2} \min_{k \in [n-1]} s_{r_k}(Z_k)$. Then, plugging in Equation (D24), one sees that one has

$$\|\hat{G}_k - G_k\|_F^2 \leq 2c_Z^2(c_G^2 r_{\max}^2 \tilde{\varepsilon}^2 + 4r_{\max}^2 \tilde{\varepsilon}^2) = 2c_Z^2 r_{\max}^2 (c_G^2 + 4) \tilde{\varepsilon}^2.$$

Thus, for Equation (D25) to hold with probability $1 - \delta$, one takes $\tilde{\varepsilon}^{-2} = 2c_Z^2 r_{\max}^2 (c_G^2 + 4) \varepsilon^{-2}$, which shows that our choice of B leads to $r_{\max} \tilde{\varepsilon} \leq \frac{1}{2} \min_{k \in [n-1]} s_{r_k}(Z_k)$ with probability $1 - \delta$. Therefore, the choice of B allows Equation (D25) to hold with probability $1 - \delta$. \square

D.4 Global error bound on estimating ρ

We have established that the tensor components $(\hat{G}_k)_{k=1}^n$ converge to $(G_k)_{k=1}^n$ at an $\mathcal{O}(B^{-1/2})$ rate when given $\mathcal{O}(B)$ copies of ρ . This subsection shows how the local component-wise convergence ensures that the final output $\tilde{\rho}$ converges to ρ . The analysis in this section uses a novel perturbational result for tensor train. This part of the error analysis heavily uses tensor reshaping, and we frequently reshape tensors into matrices. Therefore, we introduce an additional matricization notation that simplifies the analysis.

Definition 3 Let n be the dimension of an n -tensor $C: \prod_{k=1}^n [m_k] \rightarrow \mathbb{R}$, and let I, J be two non-overlapping index sets with $I \cup J = [n]$. We use $C(i_I; i_J)$ to denote the *unfolding matrix* with bipartition $I \cup J = [n]$. Namely, we group the indices in I and J respectively as the row index and column index. The matrix $C(i_I; i_J)$ is of size $(\prod_{k \in I} m_k) \times (\prod_{l \in J} m_l)$.

We present a result on how local component-wise error propagates to the global tensor train error in the Frobenius norm. To the best of our knowledge, this result is a novel contribution first derived in this work. We anticipate that this bound is of independent interest for the tensor network community. Minimal modifications would generalize the result to tree-based tensor networks as defined in [150].

Lemma 2 Let d be the dimension, and let $(F_k)_{k=1}^d$ be a series of tensor components such that $F_1 \in \mathbb{R}^{m_1 \times r_1}$, $F_k \in \mathbb{R}^{r_{k-1} \times m_k \times r_k}$ for $k = 2, \dots, d-1$, and $F_d \in \mathbb{R}^{r_{d-1} \times m_d}$. Let D be a tensor train formed by $(F_k)_{k=1}^d$ via the following equation

$$\begin{array}{c} \boxed{D} \\ | \quad | \quad \cdots \quad | \\ i_1 \quad i_2 \quad \cdots \quad i_d \end{array} = \begin{array}{c} \boxed{F_1} \text{---} \boxed{F_2} \text{---} \cdots \text{---} \boxed{F_d} \\ | \quad \quad \quad | \quad \quad \quad | \\ i_1 \quad \quad \quad i_2 \quad \quad \quad i_d \end{array}. \quad (\text{D30})$$

For $k = 1, \dots, d$, let ΔF_k be a perturbation to F_k with $\hat{F}_k = F_k + \Delta F_k$. Let \tilde{D} be a tensor train formed by $(\hat{F}_k)_{k=1}^d$ via the following equation

$$\begin{array}{c} \boxed{\tilde{D}} \\ | \quad | \quad \cdots \quad | \\ i_1 \quad i_2 \quad \cdots \quad i_d \end{array} = \begin{array}{c} \boxed{\hat{F}_1} \text{---} \boxed{\hat{F}_2} \text{---} \cdots \text{---} \boxed{\hat{F}_d} \\ | \quad \quad \quad | \quad \quad \quad | \\ i_1 \quad \quad \quad i_2 \quad \quad \quad i_d \end{array}. \quad (\text{D31})$$

We suppose that the following conditions hold:

1. For $k = 1$, one has $m_1 \geq r_1$. Moreover, the unfolding matrix $F_1(i_1; \alpha_1) \in \mathbb{R}^{m_1 \times r_1}$ is of rank r_1 .
2. For $k = 2, \dots, d-1$, one has $m_k \geq r_{k-1} r_k$. Moreover, the unfolding matrix $F_k(i_k; (\alpha_{k-1}, \alpha_k))$ is of rank $r_{k-1} r_k$.
3. For $k = d$, one has $m_d \geq r_{d-1}$. Moreover, the unfolding matrix $F_d(i_d; \alpha_{d-1}) \in \mathbb{R}^{m_d \times r_{d-1}}$ is of rank r_{d-1} .
4. There exists an $\varepsilon > 0$ so that for any $k \in [d]$, one has

$$\|F_k - \hat{F}_k\|_F \leq \varepsilon. \quad (\text{D32})$$

Under the given conditions, define a constant c_F by

$$c_F = \max \left(\|F_1(i_1; \alpha_1)^\dagger\|, \max_{k=2, \dots, d-1} \|F_k(i_k; (\alpha_{k-1}, \alpha_k))^\dagger\|, \|F_d(i_d; \alpha_{d-1})^\dagger\| \right).$$

Then, assuming that $\varepsilon \leq c_F^{-1} d^{-1}$, one has

$$\frac{\|D - \tilde{D}\|_F}{\|D\|_F} \leq 2dc_F \varepsilon.$$

Proof We first perform the analysis via a telescoping sum construction. Let $D_0 = D$, $D_d = \tilde{D}$. For $k = 1, \dots, d-1$, we let D_k be a tensor train with tensor component given by $(\hat{F}_l)_{l=1}^k \cup (F_l)_{l=k+1}^d$. In terms of the diagram, one writes

$$\begin{array}{c} \boxed{D_k} \\ i_1 \quad i_2 \quad \cdots \quad i_d \end{array} = \begin{array}{c} \boxed{\hat{F}_1} \cdots \boxed{\hat{F}_k} \boxed{F_{k+1}} \cdots \boxed{F_d} \\ i_1 \quad \quad \quad i_k \quad i_{k+1} \quad \quad \quad i_d \end{array}. \quad (\text{D33})$$

By the triangle inequality, one has

$$\|D - \tilde{D}\|_F = \|D_0 - D_d\|_F \leq \sum_{k=0}^{d-1} \|D_k - D_{k+1}\|_F.$$

For each of the difference term $\|D_k - D_{k+1}\|_F$, we define tensors $D_{<k}$, $\tilde{D}_{<k}$ by the following equations:

$$\begin{array}{c} \boxed{D_{<k}} \\ i_1 \quad \cdots \quad i_{k-1} \end{array} = \begin{array}{c} \boxed{F_1} \cdots \boxed{F_{k-1}} \\ i_1 \quad \quad \quad i_{k-1} \end{array},$$

$$\begin{array}{c} \boxed{\tilde{D}_{<k}} \\ i_1 \quad \cdots \quad i_{k-1} \end{array} = \begin{array}{c} \boxed{\hat{F}_1} \cdots \boxed{\hat{F}_{k-1}} \\ i_1 \quad \quad \quad i_{k-1} \end{array}.$$

Similarly, we define $D_{>k}$ by

$$\begin{array}{c} \boxed{D_{>k}} \\ i_{k+1} \quad \cdots \quad i_d \end{array} = \begin{array}{c} \boxed{F_{k+1}} \cdots \boxed{F_d} \\ i_{k+1} \quad \quad \quad i_d \end{array}.$$

As a result, for $k = 2, \dots, d-1$, one has

$$\begin{array}{c} \boxed{D_k} \\ i_1 \quad i_2 \quad \cdots \quad i_d \end{array} - \begin{array}{c} \boxed{D_{k-1}} \\ i_1 \quad i_2 \quad \cdots \quad i_d \end{array} = \begin{array}{c} \boxed{\tilde{D}_{<k}} \boxed{\Delta F_k} \boxed{D_{>k}} \\ i_1 \quad \cdots \quad i_{k-1} \quad i_k \quad i_{k+1} \quad \cdots \quad i_d \end{array}. \quad (\text{D34})$$

We first consider the boundary term $\|D_0 - D_1\|_F$. Similar to Equation (D34), one has

$$\begin{array}{c} \boxed{D_1} \\ i_1 \quad i_2 \quad \cdots \quad i_d \end{array} - \begin{array}{c} \boxed{D_0} \\ i_1 \quad i_2 \quad \cdots \quad i_d \end{array} = \begin{array}{c} \boxed{\Delta F_1} \boxed{D_{>1}} \\ i_1 \quad i_2 \quad \cdots \quad i_d \end{array}. \quad (\text{D35})$$

Deriving the bound for the $\|D_0 - D_1\|_F$ term in Equation (D35) is instructive, and our subsequent bound uses essentially the same technique. We let $J_1 = \{2, \dots, n\}$ and we consider the unfolding matrices $D_0(i_1; i_{J_1})$, $D_1(i_1; i_{J_1})$ and $D_{>1}(\alpha_1; i_{J_1})$. The equation in Equation (D35) reads

$$D_1(i_1; i_{J_1}) - D_0(i_1; i_{J_1}) = \Delta F_1(i_1; \alpha_1) D_{>1}(\alpha_1; i_{J_1}).$$

Let $A \in \mathbb{R}^{m \times r}$ be a matrix of rank r , and let $B \in \mathbb{R}^{r \times L}$ be a matrix where L could potentially be very large. For v being an arbitrary column of B , one has

$$\frac{\|Av\|^2}{\|v\|^2} \geq \|A^\dagger\|^{-2}.$$

By summing $\|Av\|^2 \geq \|A^\dagger\|^{-2} \|v\|^2$ over all choices of v , one has

$$\frac{\|AB\|_F}{\|B\|_F} \geq \|A^\dagger\|^{-1}.$$

Then, let ΔA be a perturbation to A with $\hat{A} = A + \Delta A$. One has

$$\|(A - \hat{A})B\|_F \leq \|(A - \hat{A})\| \|B\|_F \leq \|A^\dagger\| \|\Delta A\| \|AB\|_F.$$

In other words, for a well-conditioned matrix A , one has a relative error bound

$$\frac{\|(A - \hat{A})B\|_F}{\|AB\|_F} \leq \|A^\dagger\| \|\Delta A\|. \quad (\text{D36})$$

Then, by condition (1) in the statement of Lemma 2, we see that we can apply Equation (D36) with F_1, \hat{F}_1 in place of A, \hat{A} and with $D_{>1}(\alpha; i_{J_1})$ in place of B . One has

$$\|D_1 - D_0\|_F \leq \|\Delta F_1\| \|F_1^\dagger\| \|F_1(i_1; \alpha_1) D_{>1}(\alpha_1; i_{J_1})\|_F = \|\Delta F_1\| \|F_1^\dagger\| \|D\|_F, \quad (\text{D37})$$

where the last equality is true since the contraction between F_1 and $D_{<1}$ on the α_1 index forms D .

For $1 < k < n$, we first rewrite Equation (D34) in terms of a matrix equation. We let $J_k = \{k+1, \dots, d\}$, and then one can write

$$\begin{aligned} & D_k(i_k; (i_{[k-1]}, i_{J_k})) - D_{k-1}(i_k; (i_{[k-1]}, i_{J_k})) \\ &= \Delta F_k(i_k; (\alpha_{k-1}, \alpha_k)) \tilde{D}_{<k} \otimes D_{>k}((\alpha_{k-1}, \alpha_k); (i_{[k-1]}, i_{J_k})), \end{aligned}$$

In particular, the unfolding matrix term $\tilde{D}_{<k} \otimes D_{>k}((\alpha_{k-1}, \alpha_k); (i_{[k-1]}, i_{J_k}))$ is the Kronecker product between the two unfolding matrices $\tilde{D}_{<k}(\alpha_{k-1}; i_{[k-1]})$ and $D_{>k}(\alpha_k; i_{J_k})$. One can check that the matrix equation is equivalent to Equation (D34).

To simplify the notation, in what follows, we assume that D_{k-1}, D_k respectively represent the unfolding matrix $D_{k-1}(i_k; (i_{[k-1]}, i_{J_k})), D_k(i_k; (i_{[k-1]}, i_{J_k}))$. We assume that $F_k, \Delta F_k$ respectively represent the unfolding matrix $F_k(i_k; (\alpha_{k-1}, \alpha_k)), \Delta F_k(i_k; (\alpha_{k-1}, \alpha_k))$. We assume that $D_{<k}, \tilde{D}_{<k}$ respectively represent the unfolding matrix $D_{<k}(\alpha_{k-1}; i_{[k-1]}), \tilde{D}_{<k}(\alpha_{k-1}; i_{[k-1]})$. Likewise, we assume that $D_{>k}$ represent the unfolding matrix $D_{>k}(\alpha_k; i_{J_k})$. Then, one can write Equation (D34) compactly as the matrix equation

$$D_k - D_{k-1} = \Delta F_k (\tilde{D}_{<k} \otimes D_{>k}).$$

By the triangle inequality, we have

$$\|\Delta F_k (\tilde{D}_{<k} \otimes D_{>k})\|_F \leq \|\Delta F_k ((\tilde{D}_{<k} - D_{<k}) \otimes D_{>k})\|_F + \|\Delta F_k (D_{<k} \otimes D_{>k})\|_F. \quad (\text{D38})$$

We see that condition (2) in the statement of Lemma 2 allows us to use Equation (D36). In particular, we take $F_k, \tilde{F}_k, \Delta F_k$ to be in place of $A, \hat{A}, \Delta A$. For the place of B , we consider both $D_{<k} \otimes D_{>k}$ and $\tilde{D}_{<k} \otimes D_{>k}$.

In the first case, we take B to be $D_{<k} \otimes D_{>k}$, and we have

$$\begin{aligned} & \|\Delta F_k ((\tilde{D}_{<k} - D_{<k}) \otimes D_{>k})\|_F \\ & \leq \|\Delta F_k\| \|F_k^\dagger\| \|F_k ((\tilde{D}_{<k} - D_{<k}) \otimes D_{>k})\|_F, \\ & = \|\Delta F_k\| \|F_k^\dagger\| \|D_{k-1} - D\|_F, \end{aligned}$$

where the last equality is because the contraction between F_k and $\tilde{D}_{<k} \otimes D_{>k}$ on the (α_{k-1}, α_k) index forms D_{k-1} (see Equation (2) for a diagram illustration), whereas the contraction between F_k and $D_{<k} \otimes D_{>k}$ on the (α_{k-1}, α_k) index forms D .

Similarly, taking B to be $\tilde{D}_{<k} \otimes D_{>k}$ in Equation (D36), we have

$$\begin{aligned} & \|\Delta F_k (D_{<k} \otimes D_{>k})\|_F \\ & \leq \|\Delta F_k\| \|F_k^\dagger\| \|F_k (D_{<k} \otimes D_{>k})\|_F, \\ & = \|\Delta F_k\| \|F_k^\dagger\| \|D\|_F, \end{aligned}$$

where the last equality is because the contraction between F_k and $D_{<k} \otimes D_{>k}$ on the (α_{k-1}, α_k) index forms D .

Thus, combining the two results, we have

$$\|D_{k-1} - D_k\|_F \leq \|\Delta F_k\| \|F_k^\dagger\| (\|D_{k-1} - D\|_F + \|D\|_F). \quad (\text{D39})$$

For the case of $k = d$, by repeating the calculation in the $1 < k < d$ case, one has

$$\|D_{d-1} - D_d\|_F \leq \|\Delta F_d(i_d; \alpha_{d-1})\| \|F_d(i_d; \alpha_{d-1})^\dagger\| (\|D_{d-1} - D\|_F + \|D\|_F). \quad (\text{D40})$$

The rest of the proof is by a simple induction-type argument. We write $b_k = \|D_{k-1} - D_k\|$. One can see that Equation (D37) can be written as

$$b_1 \leq \|\Delta F_1\| \|F_1^\dagger\| \|D\|_F \leq c_F \varepsilon \|D\|_F,$$

where the last inequality uses the definition of c_F and ε in the statement of Lemma 2. Likewise, Equation (D39) shows that, for $k = 2, \dots, d-1$, one has

$$b_k \leq \|\Delta F_k\| \|F_k^\dagger\| (\|D_{k-1} - D\|_F + \|D\|_F) \leq c_F \varepsilon \left(\sum_{l=1}^{k-1} b_l + \|D\|_F \right).$$

Lastly, for $k = d$, we have

$$\begin{aligned} b_k &\leq \|\Delta F_d(i_d; \alpha_{d-1})\| \|F_d(i_d; \alpha_{d-1})^\dagger\| (\|D_{d-1} - D\|_F + \|D\|_F) \\ &\leq c_F \varepsilon \left(\sum_{l=1}^{d-1} b_l + \|D\|_F \right). \end{aligned}$$

Our induction hypothesis is that $b_k \leq c_F \varepsilon (1 + c_F \varepsilon)^{k-1} \|D\|_F$. One sees that this inequality holds when $k = 1$. Then, suppose that the statement is true for all indices up to k . Then, for $k+1$, one has

$$b_{k+1} \leq c_F \varepsilon \left(\sum_{l=1}^k b_l + \|D\|_F \right) \leq c_F \varepsilon \left(\sum_{l=1}^k \varepsilon c_F (1 + c_F \varepsilon)^{l-1} + 1 \right) \|D\|_F = c_F \varepsilon (1 + c_F \varepsilon)^k \|D\|_F,$$

where the last equality uses the formula for geometric series summation. Thus, the claim is true for $k \in [d]$.

Lastly, we plug in the telescoping sum and obtain

$$\|D - \tilde{D}\|_F \leq \sum_{k=1}^d b_k \leq \sum_{k=1}^d c_F \varepsilon (1 + c_F \varepsilon)^{k-1} \|D\|_F \leq \left((1 + c_F \varepsilon)^d - 1 \right) \|D\|_F.$$

Under the assumption that $c_F \varepsilon < 1/d$, one further has

$$\frac{\|D - \tilde{D}\|_F}{\|D\|_F} \leq \left((1 + c_F \varepsilon)^d - 1 \right) \leq e^{c_F d \varepsilon} - 1 \leq 2c_F d \varepsilon,$$

where the second inequality is due to $1+t \leq e^t$, and the third inequality is because $e^x \leq 1+2x$ for $x \in [0, 1]$. \square

One can see that Lemma 2 can not be directly applied to our setting unless the coefficient tensor C has maximal rank $r \leq 2$. However, the result in Lemma 2 becomes applicable after one merges several tensor components into a bigger tensor component. To use Lemma 2, we shall merge connected tensor components. For example, if one has L tensor components G_k, \dots, G_{k+L-1} , then merging these components leads to

$$\begin{array}{c} \boxed{F} \\ \downarrow \\ i_k \quad \cdots \quad i_{k+L-1} \end{array} = \begin{array}{c} \boxed{G_k} \cdots \boxed{G_{k+L-1}} \\ \downarrow \quad \quad \downarrow \\ i_k \quad \quad \quad i_{k+L-1} \end{array},$$

which one views as a 3-tensor of size $r_{k-1} \times 4^L \times r_{k+L-1}$. One sees that it suffices to take merge $L = \lceil \log_2(r_{\max}) \rceil$ blocks to ensure that the condition in Lemma 2 can hold.

We are now ready to prove our main result.

Proposition 5 (*Global error bound on sketch tomography*) *Assume that one is in the setting of Theorem 4. Let ε_3 be an accuracy parameter so that Algorithm 1 satisfies*

$$\max_{k \in [n]} \|G_k - \hat{G}_k\|_F \leq \varepsilon_3.$$

Suppose that r_{\max} is as in Theorem 4. We let $L = \lceil \log_2(r_{\max}) \rceil$ and we suppose that $n > L^2$. Then, there exists $a, b \in \mathbb{Z}_{\geq 0}$ so that $n = aL + b(L+1)$. For $j = 1, \dots, a$, we construct F_j to be a tensor component constructed by merging tensor components $G_{(j-1)L+1}, \dots, G_{(j-1)L+L}$. For $j = a+1, \dots, a+b$, we let F_j to be a tensor component constructed by merging tensor components $G_{aL+(j-1-a)(L+1)+1}, \dots, G_{aL+(j-1-a)(L+1)+L+1}$. Similarly, we define \hat{F}_j to be tensor components obtained by merging $(\hat{G}_k)_{k=1}^n$. Then, if $\varepsilon_3 \leq \frac{c_G}{L+1}$, one has

$$\max_{j \in [a+b]} \|F_j - \hat{F}_j\|_F \leq 2(L+1)c_G^L \varepsilon_3. \quad (\text{D41})$$

In particular, let $\varepsilon \in (0, 1)$ be an accuracy parameter and let c_S, r_{\max}, c_Z, c_G be the same terms as in Theorem 4. Moreover, let c_F be as in Lemma 2 with the definition of $(F_j)_{j=1}^{a+b}$ given as above. In Algorithm 1, set $W = 2 \log(12n\tilde{r}_{\max}^2/\delta)$ and set

$$B \geq 128n^2 c_G^{2L} c_F^2 c_S^2 r_{\max}^2 c_Z^2 (c_G^2 + 4) \varepsilon^{-2},$$

Then, with probability $1 - \delta$, one has

$$\frac{\|\tilde{\rho} - \rho\|_F}{\|\rho\|_F} \leq \varepsilon. \quad (\text{D42})$$

Proof We first prove Equation (D41). For two matrices A, B one has the simple bound

$$\|AB\|_F \leq \|A\| \|B\|_F \leq \|A\|_F \|B\|_F.$$

Therefore, for an arbitrary tensor network E consisting of tensor components $(M_k)_{k=1}^K$, one has the simple bound

$$\|E\|_F \leq \prod_{k=1}^K \|M_k\|_F, \quad (\text{D43})$$

and the inequality is quite loose in general. Moreover, let E' be a tensor network of the same tensor network structure as E , and let E' consist of tensor components $(M'_k)_{k=1}^K$. In particular, each of the tensor components M'_k is of the same shape as M_k . We claim that

$$\|E' - E\|_F \leq \sum_{S \subseteq [K], |S| > 0} \prod_{k \in S} \|M'_k - M_k\|_F \prod_{j \notin S} \|M_j\|_F. \quad (\text{D44})$$

We prove Equation (D44). Let $S \subseteq [K]$ be a nonempty subset and let E_S be the tensor network of the same tensor network structure as E . Let E_S be of tensor component $(M'_k - M_k)_{k \in S} \cup (M_j)_{j \notin S}$. By multi-linearity, one has $E' - E = \sum_{S \subseteq [K], |S| > 0} E_S$, and hence one has

$$\|E' - E\|_F \leq \sum_{S \subseteq [K], |S| > 0} \|E_S\|_F \leq \sum_{S \subseteq [K], |S| > 0} \prod_{k \in S} \|M_k - M'_k\|_F \prod_{j \notin S} \|M_j\|_F,$$

where the first inequality is by the triangle inequality, and the second inequality is by Equation (D43). In particular, if one writes $\zeta = \max_{k \in [K]} \|M_k\|_F$ and $\gamma = \max_{k \in [K]} \|M_k - M'_k\|_F$, then Equation (D44) implies

$$\|E' - E\|_F \leq \sum_{S \subseteq [K], |S| > 0} \gamma^{|S|} \zeta^{K-|S|} = (\gamma + \zeta)^K - \zeta^K,$$

where the last equality is by the binomial theorem. In particular, we consider the case where $\gamma \leq \frac{\zeta}{K}$, where one has

$$\|E' - E\|_F \leq (\gamma + \zeta)^K - \zeta^K = \zeta^K \left((1 + \gamma/\zeta)^K - 1 \right) \leq \zeta^K (\exp(\gamma K/\zeta) - 1) \leq 2\gamma K \zeta^{K-1},$$

where the second inequality is because $(1+x) \leq \exp(x)$, and the second inequality is because $\exp(x) \leq 1 + 2x$ for $x \in [0, 1]$.

We can now bound the magnitude of $\|F_j - \hat{F}_j\|_F$. We see that F_j, \hat{F}_j are two tensor networks of the same structure, and the tensor components share the same shape. There are at most $L+1$ components. Each component of F_j is bounded in the Frobenius norm by C_G , and the difference in each tensor component is likewise bounded in the Frobenius norm by ε_3 . Thus, if $\varepsilon_3 \leq \frac{c_G}{L+1}$, one has

$$\|F_j - \hat{F}_j\|_F \leq 2(L+1)c_G^L \varepsilon_3.$$

We now show that Equation (D42) holds with high probability. First, we let $\tilde{\varepsilon}$ be a parameter to be specified. We employ Theorem 4. For $B \geq 2c_S c_Z^2 r_{\max}^2 (c_G^2 + 4)\tilde{\varepsilon}^{-2}$, the following bound holds with probability $1 - \delta$:

$$\max_{k \in [n]} \|G_k - \hat{G}_k\|_F \leq \tilde{\varepsilon}.$$

Plugging in Equation (D41), for $\tilde{\varepsilon} \leq c_G/(L+1)$, one has

$$\max_{j \in [a+b]} \|\hat{F}_j - F_j\|_F \leq 2(L+1)c_G^L \tilde{\varepsilon}.$$

Let \tilde{C} denote the tensor train consisting of tensor components $(\hat{G}_k)_{k=1}^n$. One can see that C, \tilde{C} can be respectively viewed as a tensor train with tensor components $(F_j)_{j=1}^{a+b}$ and $(\hat{F}_j)_{j=1}^{a+b}$. Using Lemma 2, if $\tilde{\varepsilon} \leq \frac{1}{2}(L+1)^{-1} c_G^{-L} c_F^{-1} (a+b)^{-1}$, we see that one has

$$\|\rho - \tilde{\rho}\| = \|C - \tilde{C}\| \leq 4(a+b)c_F(L+1)c_G^L \tilde{\varepsilon} \|C\|_F \leq 8nc_F c_G^L \tilde{\varepsilon} \|\rho\|_F,$$

where the last inequality uses $\|C\|_F = \|\rho\|_F$ and $(a+b)(L+1) \leq 2n$. Thus, for Equation (D42) to hold with probability $1 - \delta$, one takes $\tilde{\varepsilon}^{-2} = 64n^2 c_F^2 c_G^{2L} \varepsilon^{-2}$. Plugging in Theorem 4, one sees that our choice of B allows Equation (D42) to hold with probability $1 - \delta$.

Lastly, the informal version in Theorem 1 holds as a consequence of Equation (D42). In particular, when ρ is the density matrix of a pure state $|\psi\rangle$, one has $\|\rho\|_F = 1$, which is why the statement in Theorem 1 does not contain a $\|\rho\|_F$ factor. \square

We give some remarks on the bound that we have obtained in Theorem 5. The c_G^L dependency is mild because one has $L = \lceil \log_2(r_{\max}) \rceil$. However, the c_G^L dependency is due to the loose bound in Equation (D43). We conjecture that a more refined analysis can improve the c_G^L dependence to an $\mathcal{O}(1)$ dependence that is independent of L . We leave a more refined analysis for future work.

Moreover, the assumption of $n \geq L^2$ is not necessary. For the regime of $L \leq n < L^2$, one is not guaranteed to write an integer less than $L^2 - L - 1$ by a weighted sum of L and $L+1$. Therefore, one would require a more complicated construction for the merging operation to construct $(F_j)_{j=1}^d$. That said, for $n \leq L^2$, one can obtain a similar result as obtained in Theorem 5, but the worst case would involve an $\mathcal{O}(c_G^{4L})$ dependence.

Appendix E Detail on maximum likelihood estimation training using MPS

E.1 Methodology

We follow the procedure to utilize the Pauli measurement data for MLE training. One has access to B unitary transformations $\{U^{(j)} \in U(2^n)\}_{j=1}^B$ and the corresponding binary measurement outcomes $b^{(j)} = (b_1^{(j)}, \dots, b_n^{(j)}) \in \{0, 1\}^n$. The j -th measurement outcome is also a state $|b^{(j)}\rangle \in \mathbb{C}^{2^n}$ by the computational basis encoding. In the MLE framework, one minimizes a negative-log-likelihood (NLL) loss defined as follows

$$\mathcal{L}(|\phi\rangle) = -\frac{1}{B} \sum_{j=1}^B \log \left(|\langle b^{(j)} | U^{(j)} |\phi\rangle|^2 \right) + \log(\langle \phi | \phi \rangle), \quad (\text{E45})$$

and $|\phi\rangle$ is optimized over an MPS class. We illustrate the key concepts in a tensor diagram. The ansatz $|\phi\rangle$ is parameterized by a collection of tensor component $(F_k)_{k=1}^n$ and the representation of $|\phi\rangle$ is as follows:

$$\begin{array}{c} \boxed{|\phi\rangle} \\ \text{\scriptsize } j_1 \quad j_2 \quad \cdots \quad j_n \end{array} = \begin{array}{c} \boxed{F_1} \quad \boxed{F_2} \quad \cdots \quad \boxed{F_n} \\ \text{\scriptsize } j_1 \quad j_2 \quad \quad \quad j_n \end{array}.$$

The normalization constant $Z = \langle \phi | \phi \rangle$ is evaluated in a tensor diagram as follows:

$$Z = \begin{array}{c} \boxed{\bar{F}_1} \quad \boxed{\bar{F}_2} \quad \cdots \quad \boxed{\bar{F}_n} \\ \boxed{F_1} \quad \boxed{F_2} \quad \cdots \quad \boxed{F_n} \\ \text{\scriptsize } j_1 \quad j_2 \quad \quad \quad j_n \end{array}. \quad (\text{E46})$$

Similarly, the evaluation of $\langle b^{(j)} | U^{(j)} |\phi\rangle$ is done in a tensor diagram. Let $U^{(j)} = \otimes_{k=1}^n U_k^{(j)}$ be the unitary transformation for the j -th measurement. One can write the diagram for the evaluation as follows:

$$\langle b^{(j)} | U^{(j)} |\phi\rangle = \begin{array}{c} b_1^{(j)} \quad b_2^{(j)} \quad \cdots \quad b_n^{(j)} \\ \boxed{U_1^{(j)}} \quad \boxed{U_2^{(j)}} \quad \cdots \quad \boxed{U_n^{(j)}} \\ \boxed{F_1} \quad \boxed{F_2} \quad \cdots \quad \boxed{F_n} \\ \text{\scriptsize } j_1 \quad j_2 \quad \quad \quad j_n \end{array}. \quad (\text{E47})$$

The diagrams in Equation (E46) and Equation (E47) show that \mathcal{L} in Equation (E45) is efficient to evaluate and differentiate against in an MPS class. For the optimization algorithm, we use a one-site DMRG approach summarized in Algorithm 2, whereby DMRG refers to the fact that the mixed canonical form has been used and that the parameter update is done sequentially.

Algorithm 2 One-site DMRG algorithm for optimizing \mathcal{L}

Require: Loss function \mathcal{L} .

Require: Current tensor component $(F_k)_{k=1}^n$.

Require: Learning rate η

```
1: while Not converged do
2:   for  $i = 1, \dots, n$  and then  $i = n, \dots, 1$  do
3:     Transform  $|\phi\rangle$  to the mixed canonical form centered at site  $i$ .
4:     Perform gradient descent update:  $F_i \leftarrow F_i - \eta \frac{\partial \mathcal{L}}{\partial F_i}$ .
5:   end for
6: end while
7: return Final tensor component  $(F_k)_{k=1}^n$ .
```

E.2 Implementation detail

We report the implementation details for our MLE benchmark. For the 1D Heisenberg experiment and the 1D TFIM experiment in the main text, we choose a learning rate of $\eta = 0.1$ and we obtain $|\phi\rangle$ by running many iterations of Algorithm 2 until $\mathcal{L}(|\phi\rangle) \leq \mathcal{L}(|\psi\rangle)$. By the definition of the loss function in the MLE procedure, this means that the obtained state $|\phi\rangle$ is better at explaining the generated data than the true state $|\psi\rangle$. The ansatz for $|\phi\rangle$ is taken to be in the same class as $|\psi\rangle$ in the sense that $|\phi\rangle$ is optimized over the complex MPS and all tensor components of $|\phi\rangle$ are of the same shape as $|\psi\rangle$.

The main text shows that the obtained MLE solution is not accurate in certain observable estimation tasks. One can conclude from the numerical performance that, for practical settings, an MPS model that is competitive in the log likelihood metric can have poor observable estimation accuracy. MLE is trained on the log likelihood metric, and it does not include a penalization term for how well it predicts individual observables. Therefore, when the sample size is not sufficiently large, the fact that $|\psi\rangle$ is successful in the log likelihood metric is insufficient to guarantee an accurate observable prediction. On the other hand, MLE training is more computationally challenging when the sample size is large. We remark that the conducted experiment is already more ideal than practical settings by using the log likelihood level of the true model $|\psi\rangle$ as a termination criterion. In practice, one might even prematurely terminate training when in a local minimum, which leads to a worse quality for the MLE solution. Therefore, while MLE is a good practical proposal for quantum state tomography, our proposed sketch tomography procedure is, in some cases, more advantageous due to its performance guarantee in Theorem 1 and due to practical performances shown in the main text.

We explain why we do not include a benchmark in the 2D Heisenberg experiment. To calculate the evaluation diagram used in Equation (E47), one needs to at least store a complex tensor of size $a \times 2 \times a$. Therefore, the memory complexity of calculating B samples in parallel is on the order of $4a^2B$ floating points. For $B = 10^4$ samples, the memory requirement is 6.4 GB, which is already quite substantial. Therefore, training the MLE model has a substantial memory complexity even for a small sample size. Moreover, as mentioned in the main text, the Pauli measurement samples for $|\psi\rangle$ are

too small and will likely lead to overfitting when one chooses $|\phi\rangle$ to be in the same MPS class as $|\psi\rangle$. Therefore, to have a fair assessment of MLE, one would also need a much larger sample size, which would drastically increase the computational complexity to perform the training. Therefore, we choose to keep the sample size at $B = 8 \times 10^5$ and only present the result for sketch tomography. For researchers who wish to train an MLE benchmark in this 2D experiment, we suggest that training the MPS model with a mini-batch stochastic gradient descent strategy might allow one to compare MLE with shadow tomography.

Appendix F Proof of the lower bound

In this section, we provide both a formal version and a complete proof of the information-theoretic lower bound presented in Theorem 2 of Section 2.2 above. We begin by presenting a mathematical definition of tensor trains as follows, which serves as a complement to the definition based on tensor diagrams presented in (2) of Section 2 above.

Definition 4 (Mathematical definition of Tensor Trains) In general, any TT $\rho \in \mathbb{C}^{2^n \times 2^n}$ associated with a quantum system of n qubits has the following form:

$$\begin{aligned} & \rho(x_1, x_2, \dots, x_n; y_1, y_2, \dots, y_n) \\ & := \sum_{\alpha_1=1}^{r_1} \cdots \sum_{\alpha_{n-1}=1}^{r_{n-1}} G_1(x_1, y_1, \alpha_1) G_2(\alpha_1, x_2, y_2, \alpha_2) \cdots G_n(\alpha_{n-1}, x_n, y_n), \end{aligned} \quad (\text{F48})$$

where $G_k \in \mathbb{R}^{r_{k-1} \times 2 \times 2 \times r_k}$ for $1 \leq k \leq n$ with $r_0 = r_n = 1$ are called the tensor components associated with the TT ρ . The vector $\mathbf{r} := (r_0, r_1, \dots, r_n)$ is said to be the ranks of the TT. Throughout this section, we use $\mathcal{M}_n(R, C)$ to denote the class of all density matrices on n qubits that admit a TT representation as in (F48) with bounded rank and Frobenius norm. Specifically,

$$\mathcal{M}_n(R, C) := \left\{ \rho \in \mathbb{C}^{2^n \times 2^n} \mid \rho \text{ is a density matrix of form (F48), } \|\rho\|_F \leq C \text{ and } r_k \leq R \text{ (} 1 \leq k \leq n-1 \text{)} \right\}. \quad (\text{F49})$$

With the formal definition of TTs given above, we then present a mathematically rigorous version of the information-theoretic lower bound as below.

Proposition 6 (Formal version of the lower bound) *Let \mathcal{U} denote the random Pauli basis measurement primitive. For any matrix product state with density matrix ρ , we take $\{\hat{\rho}_{(i)}\}_{i=1}^B$ to be the B estimations of ρ produced by applying the classical shadow protocol associated with \mathcal{U} over B measurements. Then for any constant $r \geq 2$ and estimator of ρ denoted by $\hat{\Theta} : \{\hat{\rho}_{(i)}\}_{i=1}^B \rightarrow \mathbb{C}^{2^n \times 2^n}$, we have the following minimax lower bound:*

$$\inf_{\hat{\Theta}} \sup_{\rho \in \mathcal{M}_n(r, 1)} \mathbb{E}_{\{\hat{\rho}_{(i)}\}_{i=1}^B} [\|\hat{\Theta} - \rho\|_F] \gtrsim \sqrt{\frac{n}{B}}, \quad (\text{F50})$$

under the assumption that $B \geq n$, where the notation $\mathbb{E}_{\{\hat{\rho}_{(i)}\}_{i=1}^B}[\cdot]$ above means that the expectation is taken with respect to the B estimations $\{\hat{\rho}_{(i)}\}_{i=1}^B$.

Before discussing the proof of Theorem 6 above, we need to present a few lemmas. In particular, Lemma 3 below discusses properties of the TT class specified in Definition 4 above under tensor products, while Lemma 4 provides a universal upper bound on the rank of any TT in $\mathbb{C}^{2^n \times 2^n}$.

Lemma 3 Fix integers n_1, n_2 and R_1, R_2 in \mathbb{N}^+ . Then for any two constants $C_1, C_2 \in (0, 1)$ and TTs $\rho^{(1)}, \rho^{(2)}$ satisfying $\rho^{(1)} \in \mathcal{M}_{n_1}(R_1, C_1)$ and $\rho^{(2)} \in \mathcal{M}_{n_2}(R_2, C_2)$, we have that the tensor product $\rho^{(1)} \otimes \rho^{(2)} \in \mathcal{M}_{n_1+n_2}(\max\{R_1, R_2\}, C_1 C_2)$.

Proof Note that the bound on Frobenius norm directly follows from the fact that $\|\rho^{(1)} \otimes \rho^{(2)}\|_F = \|\rho^{(1)}\|_F \|\rho^{(2)}\|_F$. Hence, it suffices to check that the tensor product $\rho^{(1)} \otimes \rho^{(2)}$ can be expressed by some TT whose ranks are all bounded by $\max\{R_1, R_2\}$. Following the notations used in (F48), we assume that the tensor components of $\rho^{(1)}$ and $\rho^{(2)}$ are given by $\{C_j\}_{j=1}^{n_1}$ and $\{D_j\}_{j=1}^{n_2}$ respectively. Specifically, the two TTs can be expressed in the form of (F48) as follows:

$$\begin{aligned} & \rho^{(1)}(x_1, x_2, \dots, x_{n_1}; y_1, y_2, \dots, y_{n_1}) \\ &:= \sum_{\alpha_1=1}^{r_1} \cdots \sum_{\alpha_{n_1-1}=1}^{r_{n_1-1}} C_1(x_1, y_1, \alpha_1) C_2(\alpha_1, x_2, y_2, \alpha_2) \cdots C_{n_1}(\alpha_{n_1-1}, x_{n_1}, y_{n_1}), \\ & \rho^{(2)}(x_1, x_2, \dots, x_{n_2}; y_1, y_2, \dots, y_{n_2}) \\ &:= \sum_{\beta_1=1}^{r'_1} \cdots \sum_{\beta_{n_2-1}=1}^{r'_{n_2-1}} D_1(x_1, y_1, \beta_1) D_2(\beta_1, x_2, y_2, \beta_2) \cdots D_{n_2}(\beta_{n_2-1}, x_{n_2}, y_{n_2}), \end{aligned} \tag{F51}$$

Now let's consider tensor components $\{E_j\}_{j=1}^{n_1+n_2}$ defined as follows:

$$\begin{aligned} E_{n_1}(\gamma, x, y, 1) &= C_{n_1}(\gamma, x, y), \quad (1 \leq \gamma \leq r_{n_1-1}, x \in \{0, 1\}, y \in \{0, 1\}) \\ E_{n_1+1}(1, x, y, \gamma) &= D_1(x, y, \gamma), \quad (1 \leq \gamma \leq r'_1, x \in \{0, 1\}, y \in \{0, 1\}) \\ E_k &= C_k \quad (1 \leq k \leq n_1 - 1), \quad E_{k'} = D_{k'-n_1} \quad (n_1 + 2 \leq k' \leq n_1 + n_2). \end{aligned} \tag{F52}$$

Then we have that the tensor product $\rho^{(1)} \otimes \rho^{(2)}$ satisfies

$$\begin{aligned} & (\rho^{(1)} \otimes \rho^{(2)})(x_1, \dots, x_{n_1}, x_{n_1+1}, \dots, x_{n_1+n_2}; y_1, \dots, y_{n_1}, y_{n_1+1}, \dots, y_{n_1+n_2}) \\ &= \rho^{(1)}(x_1, \dots, x_{n_1}; y_1, \dots, y_{n_1}) \rho^{(2)}(x_{n_1+1}, \dots, x_{n_1+n_2}; y_{n_1+1}, \dots, y_{n_1+n_2}) \\ &= \left(\sum_{\alpha_1=1}^{r_1} \cdots \sum_{\alpha_{n_1-1}=1}^{r_{n_1-1}} C_1(x_1, y_1, \alpha_1) \cdots C_{n_1}(\alpha_{n_1-1}, x_{n_1}, y_{n_1}) \right) \\ & \quad \left(\sum_{\beta_1=1}^{r'_1} \cdots \sum_{\beta_{n_2-1}=1}^{r'_{n_2-1}} D_1(x_{n_1+1}, y_{n_1+1}, \beta_1) \cdots D_{n_2}(\beta_{n_2-1}, x_{n_1+n_2}, y_{n_1+n_2}) \right) \\ &= \sum_{\gamma_1=1}^{r_1} \cdots \sum_{\gamma_{n_1-1}=1}^{r_{n_1-1}} \sum_{\gamma_{n_1}=1}^1 \sum_{\gamma_{n_1+1}=1}^{r'_1} \cdots \sum_{\gamma_{n_1+n_2-1}=1}^{r'_{n_2-1}} E_1(x_1, y_1, \gamma_1) \\ & \quad E_2(\gamma_1, x_2, y_2, \gamma_2) \cdots E_{n_1}(\gamma_{n_1+n_2-1}, x_{n_1+n_2}, y_{n_1+n_2}). \end{aligned} \tag{F53}$$

Given that $\rho^{(1)} \in \mathcal{M}_{n_1}(R_1, C_1)$ and $\rho^{(2)} \in \mathcal{M}_{n_2}(R_2, C_2)$, we have $r_j \leq R_1$ ($1 \leq j \leq n_1 - 1$) and $r'_j \leq R_2$ ($1 \leq j \leq n_2 - 1$). Then we can directly deduce that $\rho^{(1)} \otimes \rho^{(2)}$ can be expressed by some TT with ranks all bounded by $\max\{R_1, R_2\}$. This concludes our proof. \square

Lemma 4 For any fixed integer $m \in \mathbb{N}^+$ and $\rho \in \mathbb{C}^{2^m \times 2^m}$, we have $\rho \in \mathcal{M}_m(2^m, \|\rho\|_F)$

Proof From the definition of the class $\mathcal{M}_m(2^m, \|\rho\|_F)$ specified in (F49) above, we know it suffices to show that any $\rho \in \mathbb{C}^{2^m \times 2^m}$ can be expressed as a TT whose ranks are all bounded by 2^m . In fact, if we use A_k to denote the k -th unfolding matrix of ρ , where its row and column are formed by the first k sites and the last $m - k$ sites respectively, then we have that $A_k \in \mathbb{C}^{4^k \times 4^{m-k}}$ and satisfies the following bound

$$\text{rank}(A_k) \leq \min\{4^k, 4^{m-k}\} \leq \sqrt{4^m} = 2^m \quad (\text{F54})$$

Then we apply Theorem 2.1 in [151] directly to deduce that ρ can be expressed as a TT with ranks bounded by 2^m , as desired. \square

In addition to the results on TTs presented above, we also need a few results from nonparametric statistics in our proof. Specifically, we need Theorem 20 from [152], which is presented as below:

Theorem 7 (Fano's Method) *Fix an integer $M \geq 2$ and let (Ω, \mathcal{A}) be some measurable space. Given $(M + 1)$ probability measures $\{P_j\}_{j=0}^M$ satisfying $P_j \ll P_0$ for any $1 \leq j \leq M$ and*

$$\frac{1}{M} \sum_{j=1}^M D_{\text{KL}}(P_j, P_0) \leq \alpha_* \quad (\text{F55})$$

for some $\alpha_ \in (0, \infty)$. Then for all classifiers represented by some measurable function $\Psi : \Omega \rightarrow \{0, 1, 2, \dots, M\}$, the following bound holds:*

$$\max_{0 \leq j \leq M} P_j(\omega \in \Omega : \Psi(\omega) \neq j) \geq \frac{\sqrt{M}}{1 + \sqrt{M}} \left(1 - \frac{3\alpha_*}{\log(M)} - \frac{1}{2\log(M)} \right). \quad (\text{F56})$$

One other result we need here is the Varshamov-Gilbert (VG) Lemma, which is presented as Theorem 2.9 in [153].

Theorem 8 (VG Lemma) *Fix some $D \in \mathbb{N}^+$ that is divisible by 8. Then there exists a subset $\mathcal{V} = \left\{ \tau^{(0)}, \dots, \tau^{(2^{\frac{D}{8}})} \right\}$ of binary strings from the D -dimensional hypercube $\{0, 1\}^D$, such that $\tau^{(0)} = (0, 0, \dots, 0)$ and*

$$\left\| \tau^{(j)} - \tau^{(k)} \right\|_1 = \sum_{l=1}^D \left| \tau_l^{(j)} - \tau_l^{(k)} \right| \geq \frac{D}{8} \quad (\text{F57})$$

for any $0 \leq j \neq k \leq 2^{\frac{D}{8}}$.

Remark 1 Without loss of generality, above we assume that D is divisible by 8, as this only changes the previously stated lower bound up to a constant. Also, we note that the l_1 norm $\|\cdot\|_1$ above essentially measures the difference between any two binary strings, so the claim above essentially provides a way of constructing a collection of binary strings that are pairwise separated from each other.

We note that the VG lemma is also a key component in the proof of the information-theoretic lower bound established in [154], where it is employed to construct a family of pairwise-separated density matrices. Such a family, which is often referred to as a covering, plays a central role in characterizing fundamental information-theoretic limits of estimation problems from not only statistics [153] but also quantum physics [155, 156]. With all essential tools listed above, we now present a complete proof of the lower bound provided in Theorem 6 as follows.

Proof of Theorem 6 Without loss of generality, here we assume that n is some integer divisible by 8, as this will only impact the information-theoretic lower bound up to some constant. We begin by taking $\gamma = \frac{1}{1600B}$, which satisfies $\epsilon \in (0, \frac{1}{1600n})$ from the given assumption $B \geq n$. Then we consider the following two density matrices σ, ω in $\mathbb{C}^{2 \times 2}$ defined as follows:

$$\sigma = \frac{1}{2}\mathbf{I}_2 - \frac{1}{2}\sqrt{\gamma}X + \frac{1}{2}\sqrt{1-\gamma}Y, \quad \omega := \frac{1}{2}\mathbf{I}_2 + \frac{1}{2}\sqrt{\gamma}X + \frac{1}{2}\sqrt{1-\gamma}Y \quad (\text{F58})$$

Moreover, applying the VG Lemma listed in Theorem 8 above yields a collection $\mathcal{V}_n := \{\tau^{(0)}, \dots, \tau^{(2^{\frac{n}{8}})}\}$ of $(2^{\frac{n}{8}} + 1)$ binary strings in $\{0, 1\}^n$ such that

$$\|\tau^{(j)} - \tau^{(k)}\|_1 = \sum_{l=1}^n |\tau_l^{(j)} - \tau_l^{(k)}| \geq \frac{n}{8}, \quad (\text{F59})$$

holds for any $0 \leq j \neq k \leq 2^{\frac{n}{8}}$. Based on the two density matrices σ, ω and the collection \mathcal{V}_n of binary strings constructed above, we further define a density matrix $\rho^{(j)}$ in $\mathbb{C}^{n \times n}$ associated with the string $\tau^{(j)}$ for any $j \in \{0, 1, \dots, 2^{\frac{n}{8}}\}$, which takes the form of a tensor product as follows:

$$\rho^{(j)} := \left(\tau_1^{(j)}\sigma + (1 - \tau_1^{(j)})\omega\right) \otimes \dots \otimes \left(\tau_n^{(j)}\sigma + (1 - \tau_n^{(j)})\omega\right). \quad (\text{F60})$$

Let $\mathcal{C}_n := \{\rho^{(0)}, \rho^{(1)}, \dots, \rho^{(2^{\frac{n}{8}})}\}$ be the corresponding collection of density matrices defined in (F60) above. We begin by first verifying that $\mathcal{C}_n \subseteq \mathcal{M}_n(r, 1)$ for constant $r \geq 2$. On the one hand, since $\|\sigma\|_F = \|\omega\|_F = \frac{1}{2}(1 + \epsilon + 1 - \epsilon) = 1$, a direct computation of the Frobenius norm $\|\rho^{(j)}\|_F$ yields that

$$\|\rho^{(j)}\|_F = \prod_{i=1}^n \left\| \tau_i^{(j)}\sigma + (1 - \tau_i^{(j)})\omega \right\|_F = 1, \quad (\text{F61})$$

for any $0 \leq j \leq 2^{\frac{L}{8}}$. On the other hand, we apply Lemma 4 to the i -th component $\tau_i^{(j)}\sigma + (1 - \tau_i^{(j)})\omega$ in the tensor product $\rho^{(j)}$ to deduce that

$$\tau_i^{(j)}\sigma + (1 - \tau_i^{(j)})\omega \in \mathcal{M}_1(2, 1) \subset \mathcal{M}_1(r, 1), \quad (\text{F62})$$

for any $0 \leq j \leq 2^{\frac{L}{8}}$ and $1 \leq i \leq L$. Then we may further apply Lemma 3 to the tensor product $\rho^{(j)} = (\tau_1^{(j)}\sigma + (1 - \tau_1^{(j)})\omega) \otimes \cdots \otimes (\tau_L^{(j)}\sigma + (1 - \tau_L^{(j)})\omega)$ to deduce that $\rho^{(j)} \in \mathcal{M}_{1 \times n}(r, 1) = \mathcal{M}_n(r, 1)$ for any $0 \leq j \leq 2^{\frac{L}{8}}$, as desired.

Now we proceed to verify that density matrices in the class \mathcal{C}_n are pairwise separated before applying Fano's method. Specifically, for any $0 \leq j \neq k \leq 2^{\frac{L}{8}}$, we may compute the Frobenius norm of the difference $\rho^{(j)} - \rho^{(k)}$ as below:

$$\begin{aligned} \|\rho^{(j)} - \rho^{(k)}\|_F^2 &= \langle \rho^{(j)} - \rho^{(k)}, \rho^{(j)} - \rho^{(k)} \rangle_F \\ &= \|\rho^{(j)}\|_F^2 + \|\rho^{(k)}\|_F^2 - 2\langle \rho^{(j)}, \rho^{(k)} \rangle_F = 2 - 2\langle \rho^{(j)}, \rho^{(k)} \rangle_F \\ &= 2 - 2 \prod_{i=1}^n \langle \tau_i^{(j)}\sigma + (1 - \tau_i^{(j)})\omega, \tau_i^{(k)}\sigma + (1 - \tau_i^{(k)})\omega \rangle_F \\ &= 2 - 2\langle \sigma, \omega \rangle_F^{\|\tau^{(j)} - \tau^{(k)}\|_1}. \end{aligned} \quad (\text{F63})$$

Plugging in the expressions of σ and ω in (F58) above gives us that

$$\langle \sigma, \omega \rangle_F = \frac{1}{2} - \frac{1}{2}\gamma + \frac{1}{2}(1 - \gamma) = 1 - \gamma \quad (\text{F64})$$

Then we may substitute (F64) and the lower bound in (F59) into (F63), which yields the following lower bound

$$\|\rho^{(j)} - \rho^{(k)}\|_F^2 \geq 2 - 2(1 - \gamma)^{\frac{n}{8}} \geq 2 \times \frac{1}{2} \times \gamma \times \frac{n}{8} \geq \frac{\gamma n}{8}, \quad (\text{F65})$$

where the second last inequality follows from the assumption $B \geq n$ and the fact that

$$1 - (1 - t)^n \geq nt - \frac{n(n-1)}{2}t^2 \geq \frac{1}{2}nt$$

holds for any $n \in \mathbb{N}$ and $t \in (0, \frac{1}{n}]$. Then we can define $\delta := \sqrt{\frac{\gamma n}{8}}$ to be the separation distance between any two density matrices.

Furthermore, we now consider the probability distributions associated with the samples obtained by measuring the collection \mathcal{C}_n of pairwise separated density matrices via the classical shadow protocol based on \mathcal{U} . Specifically, we use the binary string $b_k^{(j)} = (b_k^{(j)}(l))_{l=1}^n \in \{0, 1\}^n$ to denote the outcome obtained from the k -th measurement of the density matrix $\rho^{(j)}$ under the classical shadow protocol based on \mathcal{U} for

any $1 \leq k \leq B$. From the tensor product structure of each $\rho^{(j)}$ in \mathcal{C}_n , we can deduce that the joint distribution formed by $\left\{b_k^{(j)}\right\}_{k=1}^B$ satisfies

$$P_j := \prod_{k=1}^B P_{b_k^{(j)}} = \prod_{k=1}^B \prod_{l=1}^n P_{b_k^{(j)}(l)} \quad (\text{F66})$$

for any $0 \leq j \leq 2^{\frac{L}{8}}$. Then a direct computation further implies

$$\begin{aligned} D_{\text{KL}}(P_j, P_0) &= D_{\text{KL}}\left(\prod_{k=1}^B \prod_{l=1}^n P_{b_k^{(j)}(l)}, \prod_{k=1}^B \prod_{l=1}^n P_{b_k^{(0)}(l)}\right) \\ &= \sum_{k=1}^B \sum_{l=1}^n D_{\text{KL}}\left(P_{b_k^{(j)}(l)}, P_{b_k^{(0)}(l)}\right). \end{aligned} \quad (\text{F67})$$

From our construction of the density matrices $\rho^{(j)}$ ($1 \leq j \leq 2^{\frac{L}{8}}$) given above, we have that each $P_{b_k^{(j)}(l)}$ must be a Bernoulli distribution. Moreover, we note that the difference between $\rho^{(j)}$ and $\rho^{(0)}$ is determined by the difference between σ and ω for any $1 \leq j \leq 2^{\frac{n}{8}}$. By using $\text{Ber}(p)$ to denote the Bernoulli distribution with mean p for any $p \in (0, 1)$, we can use the expressions of σ and ω given in (F58) above to deduce that $D_{\text{KL}}\left(P_{b_k^{(j)}(l)}, P_{b_k^{(0)}(l)}\right)$ can be upper bounded as follows

$$\begin{aligned} D_{\text{KL}}\left(P_{b_k^{(j)}(l)}, P_{b_k^{(0)}(l)}\right) &\leq D_{\text{KL}}\left(\text{Ber}\left(\frac{1+\sqrt{\gamma}}{2}\right), \text{Ber}\left(\frac{1-\sqrt{\gamma}}{2}\right)\right) \\ &= \frac{1+\sqrt{\gamma}}{2} \log\left(\frac{\frac{1+\sqrt{\gamma}}{2}}{\frac{1-\sqrt{\gamma}}{2}}\right) + \frac{1-\sqrt{\gamma}}{2} \log\left(\frac{\frac{1-\sqrt{\gamma}}{2}}{\frac{1+\sqrt{\gamma}}{2}}\right) \\ &= \sqrt{\gamma} \log\left(\frac{1+\sqrt{\gamma}}{1-\sqrt{\gamma}}\right) \leq \frac{2\gamma}{1-\gamma} \leq 4\gamma, \end{aligned} \quad (\text{F68})$$

where the second last inequality above follows from the fact that $\log\left(\frac{1+t}{1-t}\right) \leq \frac{2t}{1-t^2}$ for $t \in (-1, 1)$ and the last inequality above follows from our choice of γ . Substituting the upper bound derived above into (F67) then yields that

$$\frac{1}{2^{\frac{n}{8}}} \sum_{j=1}^{2^{\frac{n}{8}}} D_{\text{KL}}(P_j, P_0) \leq 4nB\gamma = \frac{n}{400}. \quad (\text{F69})$$

By letting $\mathcal{B} := \{\hat{\rho}_{(i)}\}_{i=1}^B$ be the collection of B outcomes obtained via the B measurements under the classical shadow protocol and taking $\alpha^* := \frac{n}{400}$, $M := 2^{\frac{n}{8}}$ here, we can further apply Fano's method listed in Theorem 7 above to deduce the following lower

bound on the probability of misclassification for any classifier $\Theta : \mathcal{B} \rightarrow \{0, 1, \dots, M\}$:

$$\begin{aligned} \max_{0 \leq j \leq M} P_j(\Theta(\mathcal{B}) \neq j) &\geq \frac{2^{\frac{n}{16}}}{1 + 2^{\frac{n}{16}}} \left(1 - \frac{3n}{400 \times \frac{n}{8} \log(2)} - \frac{1}{\frac{n}{2} \log(2)} \right) \\ &\geq \frac{1}{2} \left(1 - \frac{3}{50 \log(2)} - \frac{1}{2 \log(2)} \right) \geq \frac{1}{20} \end{aligned} \quad (\text{F70})$$

where the second last inequality above follows from the assumption $n \geq 8$.

Finally, we will prove the desired minimax lower bound by combining the lower bound on the misclassification probability proved in (F70) above with Markov's inequality and inequality (F65) proved earlier. Specifically, for any estimator $\hat{\Theta} : \{\hat{\rho}_{(i)}\}_{i=1}^B \rightarrow \mathbb{C}^{2^n \times 2^n}$ of the target density matrix, we define a corresponding classifier $\tilde{\Theta} : \mathcal{B} \rightarrow \{0, 1, \dots, M\}$ as follows:

$$\tilde{\Theta} \in \arg \min_{0 \leq j \leq M} \left\| \hat{\Theta} - \rho^{(j)} \right\|_F \quad (\text{F71})$$

Given that the collection $\mathcal{C}_n = \{\rho^{(j)}\}_{j=0}^M$ has been proved to be δ -separated in (F63), we then have the following inequality for any $0 \leq j \leq M$:

$$P_j(\tilde{\Theta}(\mathcal{B}) \neq j) \leq P_j\left(\left\| \hat{\Theta} - \rho^{(j)} \right\|_F \geq \frac{\delta}{2}\right) \quad (\text{F72})$$

from the triangle inequality. Applying Markov's inequality to the RHS above and the lower bound in (F70) to the LHS above further implies

$$\begin{aligned} \max_{0 \leq j \leq M} \frac{\mathbb{E}_{P_j} \left[\left\| \hat{\Theta} - \rho^{(j)} \right\|_F \right]}{\frac{\delta}{2}} &\geq \max_{0 \leq j \leq M} P_j \left(\left\| \hat{\Theta} - \rho^{(j)} \right\|_F \geq \frac{\delta}{2} \right) \\ &\geq \max_{0 \leq j \leq M} P_j(\tilde{\Theta}(\mathcal{B}) \neq j) \geq \frac{1}{20}. \end{aligned} \quad (\text{F73})$$

Finally, plugging in (F73) indicates that

$$\begin{aligned} \inf_{\hat{\Theta}} \sup_{\rho \in \mathcal{M}_n(r,1)} \mathbb{E}_{\{\hat{\rho}_{(i)}\}_{i=1}^B} \left[\left\| \hat{\Theta} - \rho \right\|_F \right] &\geq \inf_{\hat{\Theta}} \max_{0 \leq j \leq M} \mathbb{E}_{P_j} \left[\left\| \hat{\Theta} - \rho^{(j)} \right\|_F \right] \\ &\geq \frac{\delta}{40} = \frac{1}{40} \sqrt{\frac{\gamma n}{8}} \gtrsim \sqrt{n\gamma} \gtrsim \sqrt{\frac{n}{B}}, \end{aligned} \quad (\text{F74})$$

as desired. This concludes our proof of the information-theoretic lower bound.

Remark 2 In order to obtain the lower bound on the number of measurements presented in Theorem 2 above, we can set $\epsilon = \sqrt{\frac{n}{B}}$ to be the lower bound proved in Theorem 6 here. Solving for the number of measurements then yields $B = \frac{n}{\epsilon^2}$. Moreover, we note that the proof strategy adopted here is similar to that of [154], which mainly relies on standard tools such

as Fano’s method and the VG lemma from nonparametric statistics. An alternative way to establish lower bounds of similar form is to follow ideas used in prior studies like [7, 156–159] by leveraging tools from quantum information theory, which we leave as future work.

References

- [1] Vogel, K., Risken, H.: Determination of quasiprobability distributions in terms of probability distributions for the rotated quadrature phase. *Physical Review A* **40**(5), 2847 (1989)
- [2] Leonhardt, U.: Quantum-state tomography and discrete wigner function. *Physical review letters* **74**(21), 4101 (1995)
- [3] Cramer, M., Plenio, M.B., Flammia, S.T., Somma, R., Gross, D., Bartlett, S.D., Landon-Cardinal, O., Poulin, D., Liu, Y.-K.: Efficient quantum state tomography. *Nature communications* **1**(1), 149 (2010)
- [4] Torlai, G., Mazzola, G., Carrasquilla, J., Troyer, M., Melko, R., Carleo, G.: Neural-network quantum state tomography. *Nature physics* **14**(5), 447–450 (2018)
- [5] White, S.R.: Density matrix formulation for quantum renormalization groups. *Physical review letters* **69**(19), 2863 (1992)
- [6] Glasser, I., Sweke, R., Pancotti, N., Eisert, J., Cirac, I.: Expressive power of tensor-network factorizations for probabilistic modeling. *Advances in neural information processing systems* **32** (2019)
- [7] Huang, H.-Y., Kueng, R., Preskill, J.: Predicting many properties of a quantum system from very few measurements. *Nature Physics* **16**(10), 1050–1057 (2020)
- [8] Landon-Cardinal, O., Liu, Y.-K., Poulin, D.: Efficient direct tomography for matrix product states. *arXiv preprint arXiv:1002.4632* (2010)
- [9] Nemirovskij, A.S., Yudin, D.B.: Problem complexity and method efficiency in optimization (1983)
- [10] Struchalin, G., Zagorovskii, Y.A., Kovlakov, E., Straupe, S., Kulik, S.: Experimental estimation of quantum state properties from classical shadows. *PRX quantum* **2**(1), 010307 (2021)
- [11] Fishman, M., White, S., Stoudenmire, E.M.: The itensor software library for tensor network calculations. *SciPost Physics Codebases*, 004 (2022)
- [12] Carrasquilla, J., Torlai, G., Melko, R.G., Aolita, L.: Reconstructing quantum states with generative models. *Nature Machine Intelligence* **1**(3), 155–161 (2019)

- [13] Hackbusch, W., Kühn, S.: A new scheme for the tensor representation. *Journal of Fourier analysis and applications* **15**(5), 706–722 (2009)
- [14] Aaronson, S.: Shadow tomography of quantum states. In: *Proceedings of the 50th Annual ACM SIGACT Symposium on Theory of Computing*, pp. 325–338 (2018)
- [15] Guță, M., Kahn, J., Kueng, R., Tropp, J.A.: Fast state tomography with optimal error bounds. *Journal of Physics A: Mathematical and Theoretical* **53**(20), 204001 (2020)
- [16] Hu, H.-Y., Choi, S., You, Y.-Z.: Classical shadow tomography with locally scrambled quantum dynamics. *Physical Review Research* **5**(2), 023027 (2023)
- [17] Akhtar, A.A., Hu, H.-Y., You, Y.-Z.: Scalable and flexible classical shadow tomography with tensor networks. *Quantum* **7**, 1026 (2023)
- [18] Bertoni, C., Haferkamp, J., Hinsche, M., Ioannou, M., Eisert, J., Pashayan, H.: Shallow shadows: Expectation estimation using low-depth random clifford circuits. *Physical Review Letters* **133**(2), 020602 (2024)
- [19] Mirzaee, M., Rezaee, M., Jafarizadeh, M.: Finite quantum tomography and semidefinite programming. *International Journal of Theoretical Physics* **46**(6), 1471–1494 (2007)
- [20] Gross, D., Liu, Y.-K., Flammia, S.T., Becker, S., Eisert, J.: Quantum state tomography via compressed sensing. *Physical review letters* **105**(15), 150401 (2010)
- [21] Liu, Y.-K.: Universal low-rank matrix recovery from pauli measurements. *Advances in Neural Information Processing Systems* **24** (2011)
- [22] Alquier, P., Butucea, C., Hebiri, M., Meziani, K., Morimae, T.: Rank-penalized estimation of a quantum system. *Physical Review A—Atomic, Molecular, and Optical Physics* **88**(3), 032113 (2013)
- [23] Gonçalves, D.S., Lavor, C., Gomes-Ruggiero, M.A., Cesário, A.T., Vianna, R.O., Maciel, T.O.: Quantum state tomography with incomplete data: Maximum entropy and variational quantum tomography. *Physical Review A—Atomic, Molecular, and Optical Physics* **87**(5), 052140 (2013)
- [24] Wang, Y.: Asymptotic equivalence of quantum state tomography and noisy matrix completion. *The Annals of Statistics* **41**(5), 2462–2504 (2013)
- [25] Kaley, A., Kosut, R.L., Deutsch, I.H.: Quantum tomography protocols with positivity are compressed sensing protocols. *npj Quantum Information* **1**(1), 1–6 (2015)

- [26] Kueng, R., Zhu, H., Gross, D.: Low rank matrix recovery from clifford orbits. arXiv preprint arXiv:1610.08070 (2016)
- [27] Kueng, R., Rauhut, H., Terstiege, U.: Low rank matrix recovery from rank one measurements. *Applied and Computational Harmonic Analysis* **42**(1), 88–116 (2017)
- [28] Kyrillidis, A., Kalev, A., Park, D., Bhojanapalli, S., Caramanis, C., Sanghavi, S.: Provable compressed sensing quantum state tomography via non-convex methods. *npj Quantum Information* **4**(1), 36 (2018)
- [29] Gupta, R., Xia, R., Levine, R.D., Kais, S.: Maximal entropy approach for quantum state tomography. *PRX Quantum* **2**(1), 010318 (2021)
- [30] Gupta, R., Sajjan, M., Levine, R.D., Kais, S.: Variational approach to quantum state tomography based on maximal entropy formalism. *Physical Chemistry Chemical Physics* **24**(47), 28870–28877 (2022)
- [31] Kim, J.L., Kollias, G., Kalev, A., Wei, K.X., Kyrillidis, A.: Fast quantum state reconstruction via accelerated non-convex programming. In: *Photonics*, vol. 10, p. 116 (2023). MDPI
- [32] Wang, Y., Liu, L., Cheng, S., Li, L., Chen, J.: Efficient factored gradient descent algorithm for quantum state tomography. *Physical Review Research* **6**(3), 033034 (2024)
- [33] Hsu, M.-C., Kuo, E.-J., Yu, W.-H., Cai, J.-F., Hsieh, M.-H.: Quantum state tomography via nonconvex riemannian gradient descent. *Physical Review Letters* **132**(24), 240804 (2024)
- [34] Schreiber, F.J., Eisert, J., Meyer, J.J.: Tomography of parametrized quantum states. *PRX Quantum* **6**(2), 020346 (2025)
- [35] Candes, E.J., Romberg, J.K., Tao, T.: Stable signal recovery from incomplete and inaccurate measurements. *Communications on Pure and Applied Mathematics: A Journal Issued by the Courant Institute of Mathematical Sciences* **59**(8), 1207–1223 (2006)
- [36] Donoho, D.L.: For most large underdetermined systems of linear equations the minimal l_1 -norm solution is also the sparsest solution. *Communications on Pure and Applied Mathematics: A Journal Issued by the Courant Institute of Mathematical Sciences* **59**(6), 797–829 (2006)
- [37] Donoho, D.L.: Compressed sensing. *IEEE Transactions on information theory* **52**(4), 1289–1306 (2006)
- [38] Candès, E.J., Wakin, M.B.: An introduction to compressive sampling. *IEEE*

signal processing magazine **25**(2), 21–30 (2008)

- [39] Ohliger, M., Nesme, V., Eisert, J.: Efficient and feasible state tomography of quantum many-body systems. *New Journal of Physics* **15**(1), 015024 (2013)
- [40] Hübener, R., Mari, A., Eisert, J.: Wick’s theorem for matrix product states. *Physical Review Letters* **110**(4), 040401 (2013)
- [41] Baumgratz, T., Nüßeler, A., Cramer, M., Plenio, M.B.: A scalable maximum likelihood method for quantum state tomography. *New Journal of Physics* **15**(12), 125004 (2013)
- [42] Haack, G., Steffens, A., Eisert, J., Hübener, R.: Continuous matrix product state tomography of quantum transport experiments. *New Journal of Physics* **17**(11), 113024 (2015)
- [43] Ran, S.-J., Sun, Z.-Z., Fei, S.-M., Su, G., Lewenstein, M.: Tensor network compressed sensing with unsupervised machine learning. *Physical Review Research* **2**(3), 033293 (2020)
- [44] Wang, J., Han, Z.-Y., Wang, S.-B., Li, Z., Mu, L.-Z., Fan, H., Wang, L.: Scalable quantum tomography with fidelity estimation. *Physical Review A* **101**(3), 032321 (2020)
- [45] Lidiak, A., Jameson, C., Qin, Z., Tang, G., Wakin, M.B., Zhu, Z., Gong, Z.: Quantum state tomography with tensor train cross approximation. *arXiv preprint arXiv:2207.06397* (2022)
- [46] Qin, Z., Jameson, C., Gong, Z., Wakin, M.B., Zhu, Z.: Quantum state tomography for matrix product density operators. *IEEE Transactions on Information Theory* **70**(7), 5030–5056 (2024)
- [47] Teng, Y., Samajdar, R., Van Kirk, K., Wilde, F., Sachdev, S., Eisert, J., Sweke, R., Najafi, K.: Learning topological states from randomized measurements using variational tensor network tomography. *arXiv preprint arXiv:2406.00193* (2024)
- [48] Landon-Cardinal, O., Poulin, D.: Practical learning method for multi-scale entangled states. *New Journal of Physics* **14**(8), 085004 (2012)
- [49] Carleo, G., Troyer, M.: Solving the quantum many-body problem with artificial neural networks. *Science* **355**(6325), 602–606 (2017)
- [50] Choo, K., Carleo, G., Regnault, N., Neupert, T.: Symmetries and many-body excitations with neural-network quantum states. *Physical review letters* **121**(16), 167204 (2018)
- [51] Park, C.-Y., Kastoryano, M.J.: Geometry of learning neural quantum states. *Physical Review Research* **2**(2), 023232 (2020)

- [52] Pei, M.Y., Clark, S.R.: Compact neural-network quantum state representations of jastrow and stabilizer states. *Journal of Physics A: Mathematical and Theoretical* **54**(40), 405304 (2021)
- [53] Koutnỳ, D., Motka, L., Hradil, Z., Řeháček, J., Sánchez-Soto, L.L.: Neural-network quantum state tomography. *Physical Review A* **106**(1), 012409 (2022)
- [54] Pescia, G., Han, J., Lovato, A., Lu, J., Carleo, G.: Neural-network quantum states for periodic systems in continuous space. *Physical Review Research* **4**(2), 023138 (2022)
- [55] Chen, A., Heyl, M.: Efficient optimization of deep neural quantum states toward machine precision. *arXiv preprint arXiv:2302.01941* (2023)
- [56] Huang, H.-Y., Kueng, R., Torlai, G., Albert, V.V., Preskill, J.: Provably efficient machine learning for quantum many-body problems. *Science* **377**(6613), 3333 (2022)
- [57] Chen, Z., Newhouse, L., Chen, E., Luo, D., Soljacic, M.: Antn: Bridging autoregressive neural networks and tensor networks for quantum many-body simulation. *Advances in neural information processing systems* **36**, 450–476 (2023)
- [58] Ibarra-García-Padilla, E., Lange, H., Melko, R.G., Scalettar, R.T., Carrasquilla, J., Bohrdt, A., Khatami, E.: Autoregressive neural quantum states of fermi hubbard models. *Physical Review Research* **7**(1), 013122 (2025)
- [59] Ahmed, S., Sanchez Munoz, C., Nori, F., Kockum, A.F.: Quantum state tomography with conditional generative adversarial networks. *Physical review letters* **127**(14), 140502 (2021)
- [60] Haah, J., Harrow, A.W., Ji, Z., Wu, X., Yu, N.: Sample-optimal tomography of quantum states. In: *Proceedings of the Forty-eighth Annual ACM Symposium on Theory of Computing*, pp. 913–925 (2016)
- [61] O’Donnell, R., Wright, J.: Efficient quantum tomography. In: *Proceedings of the Forty-eighth Annual ACM Symposium on Theory of Computing*, pp. 899–912 (2016)
- [62] O’Donnell, R., Wright, J.: Efficient quantum tomography ii. In: *Proceedings of the 49th Annual ACM SIGACT Symposium on Theory of Computing*, pp. 962–974 (2017)
- [63] Fiurášek, J.: Maximum-likelihood estimation of quantum measurement. *Physical Review A* **64**(2), 024102 (2001)
- [64] D’Ariano, G.M., Maccone, L., Presti, P.L.: Quantum calibration of measurement

- instrumentation. *Physical review letters* **93**(25), 250407 (2004)
- [65] Lundeen, J.S., Feito, A., Coldenstrodt-Ronge, H., Pregnell, K.L., Silberhorn, C., Ralph, T.C., Eisert, J., Plenio, M.B., Walmsley, I.A.: Tomography of quantum detectors. *Nature Physics* **5**(1), 27–30 (2009)
 - [66] Feito, A., Lundeen, J., Coldenstrodt-Ronge, H., Eisert, J., Plenio, M.B., Walmsley, I.A.: Measuring measurement: theory and practice. *New Journal of Physics* **11**(9), 093038 (2009)
 - [67] Cattaneo, M., Rossi, M.A., Korhonen, K., Borrelli, E.-M., García-Pérez, G., Zimborás, Z., Cavalcanti, D.: Self-consistent quantum measurement tomography based on semidefinite programming. *Physical Review Research* **5**(3), 033154 (2023)
 - [68] Zambrano, L., Ramos-Calderer, S., Kueng, R.: Fast quantum measurement tomography with dimension-optimal error bounds. *arXiv preprint arXiv:2507.04500* (2025)
 - [69] Surawy-Stepney, T., Kahn, J., Kueng, R., Guta, M.: Projected least-squares quantum process tomography. *Quantum* **6**, 844 (2022)
 - [70] Torlai, G., Wood, C.J., Acharya, A., Carleo, G., Carrasquilla, J., Aolita, L.: Quantum process tomography with unsupervised learning and tensor networks. *Nature Communications* **14**(1), 2858 (2023)
 - [71] Huang, H.-Y., Chen, S., Preskill, J.: Learning to predict arbitrary quantum processes. *PRX Quantum* **4**(4), 040337 (2023)
 - [72] Levy, R., Luo, D., Clark, B.K.: Classical shadows for quantum process tomography on near-term quantum computers. *Physical Review Research* **6**(1), 013029 (2024)
 - [73] Qin, Z., Jameson, C., Goldar, A., Wakin, M.B., Gong, Z., Zhu, Z.: Sample-efficient quantum state tomography for structured quantum states in one dimension. *arXiv preprint arXiv:2410.02583* (2024)
 - [74] Kuzmin, S., Mikhailova, V., Dyakonov, I., Straupe, S.: Learning the tensor network model of a quantum state using a few single-qubit measurements. *Physical Review A* **109**(5), 052616 (2024)
 - [75] Qin, Z., Lukens, J.M., Kirby, B.T., Zhu, Z.: Enhancing quantum state reconstruction with structured classical shadows. *npj Quantum Information* **11**(1), 147 (2025)
 - [76] Verstraete, F., Murg, V., Cirac, J.I.: Matrix product states, projected entangled pair states, and variational renormalization group methods for quantum spin

- systems. *Advances in physics* **57**(2), 143–224 (2008)
- [77] Orús, R.: A practical introduction to tensor networks: Matrix product states and projected entangled pair states. *Annals of physics* **349**, 117–158 (2014)
 - [78] Chan, G.K., Keselman, A., Nakatani, N., Li, Z., White, S.R.: Matrix product operators, matrix product states, and ab initio density matrix renormalization group algorithms. *The Journal of chemical physics* **145**(1) (2016)
 - [79] Orús, R.: Tensor networks for complex quantum systems. *Nature Reviews Physics* **1**(9), 538–550 (2019)
 - [80] Sandvik, A.W., Vidal, G.: Variational quantum monte carlo simulations with tensor-network states. *Physical review letters* **99**(22), 220602 (2007)
 - [81] Wouters, S., Verstichel, B., Van Neck, D., Chan, G.K.-L.: Projector quantum monte carlo with matrix product states. *Physical Review B* **90**(4), 045104 (2014)
 - [82] Yu, Z., Zhang, S., Khoo, Y.: Re-anchoring quantum monte carlo with tensor-train sketching. *arXiv preprint arXiv:2411.07194* (2024)
 - [83] Jiang, T., O’Gorman, B., Mahajan, A., Lee, J.: Unbiasing fermionic auxiliary-field quantum monte carlo with matrix product state trial wavefunctions. *Physical Review Research* **7**(1), 013038 (2025)
 - [84] Khoromskaia, V., Khoromskij, B., Schneider, R.: Qtt representation of the hartree and exchange operators in electronic structure calculations. *Computational methods in applied mathematics* **11**(3) (2011)
 - [85] Jolly, N., Fernández, Y.N., Waintal, X.: Tensorized orbitals for computational chemistry. *Physical Review B* **111**(24), 245115 (2025)
 - [86] Wall, M.L., Carr, L.D.: Out-of-equilibrium dynamics with matrix product states. *New Journal of Physics* **14**(12), 125015 (2012)
 - [87] Schröder, F.A., Chin, A.W.: Simulating open quantum dynamics with time-dependent variational matrix product states: Towards microscopic correlation of environment dynamics and reduced system evolution. *Physical Review B* **93**(7), 075105 (2016)
 - [88] Greene, S.M., Batista, V.S.: Tensor-train split-operator fourier transform (ttsoft) method: Multidimensional nonadiabatic quantum dynamics. *Journal of chemical theory and computation* **13**(9), 4034–4042 (2017)
 - [89] Leviatan, E., Pollmann, F., Bardarson, J.H., Huse, D.A., Altman, E.: Quantum thermalization dynamics with matrix-product states. *arXiv preprint arXiv:1702.08894* (2017)

- [90] Strathearn, A., Kirton, P., Kilda, D., Keeling, J., Lovett, B.W.: Efficient non-markovian quantum dynamics using time-evolving matrix product operators. *Nature communications* **9**(1), 3322 (2018)
- [91] Borrelli, R.: Density matrix dynamics in twin-formulation: An efficient methodology based on tensor-train representation of reduced equations of motion. *The Journal of Chemical Physics* **150**(23) (2019)
- [92] Baiardi, A., Reiher, M.: Large-scale quantum dynamics with matrix product states. *Journal of chemical theory and computation* **15**(6), 3481–3498 (2019)
- [93] Luchnikov, I., Vintskevich, S., Ouerdane, H., Filippov, S.: Simulation complexity of open quantum dynamics: Connection with tensor networks. *Physical review letters* **122**(16), 160401 (2019)
- [94] Borrelli, R., Dolgov, S.: Expanding the range of hierarchical equations of motion by tensor-train implementation. *The Journal of Physical Chemistry B* **125**(20), 5397–5407 (2021)
- [95] Ye, E., Chan, G.K.: Constructing tensor network influence functionals for general quantum dynamics. *The Journal of Chemical Physics* **155**(4) (2021)
- [96] Soley, M.B., Bergold, P., Gorodetsky, A.A., Batista, V.S.: Functional tensor-train chebyshev method for multidimensional quantum dynamics simulations. *Journal of Chemical Theory and Computation* **18**(1), 25–36 (2021)
- [97] Dunnett, A.J., Chin, A.W.: Efficient bond-adaptive approach for finite-temperature open quantum dynamics using the one-site time-dependent variational principle for matrix product states. *Physical Review B* **104**(21), 214302 (2021)
- [98] Gelß, P., Klein, R., Matera, S., Schmidt, B.: Solving the time-independent schrödinger equation for chains of coupled excitons and phonons using tensor trains. *The Journal of Chemical Physics* **156**(2) (2022)
- [99] Lyu, N., Soley, M.B., Batista, V.S.: Tensor-train split-operator ksl (tt-soksl) method for quantum dynamics simulations. *Journal of Chemical Theory and Computation* **18**(6), 3327–3346 (2022)
- [100] Ren, J., Li, W., Jiang, T., Wang, Y., Shuai, Z.: Time-dependent density matrix renormalization group method for quantum dynamics in complex systems. *Wiley Interdisciplinary Reviews: Computational Molecular Science* **12**(6), 1614 (2022)
- [101] Mangaud, E., Jaouadi, A., Chin, A., Desouter-Lecomte, M.: Survey of the hierarchical equations of motion in tensor-train format for non-markovian quantum dynamics. *The European Physical Journal Special Topics* **232**(12), 1847–1869 (2023)

- [102] Shinaoka, H., Wallerberger, M., Murakami, Y., Nogaki, K., Sakurai, R., Werner, P., Kauch, A.: Multiscale space-time ansatz for correlation functions of quantum systems based on quantum tensor trains. *Physical Review X* **13**(2), 021015 (2023)
- [103] Lyu, N., Mulvihill, E., Soley, M.B., Geva, E., Batista, V.S.: Tensor-train thermo-field memory kernels for generalized quantum master equations. *Journal of Chemical Theory and Computation* **19**(4), 1111–1129 (2023)
- [104] Liu, Z., Lyu, N., Hu, Z., Zeng, H., Batista, V.S., Sun, X.: Benchmarking various nonadiabatic semiclassical mapping dynamics methods with tensor-train thermo-field dynamics. *The Journal of Chemical Physics* **161**(2) (2024)
- [105] Grimm, R.T., Eaves, J.D.: Accurate numerical simulations of open quantum systems using spectral tensor trains. *The Journal of Chemical Physics* **161**(23) (2024)
- [106] Chen, G., Lado, J.L., Song, F.: Many-body liouvillian dynamics with a non-hermitian tensor-network kernel polynomial algorithm. *Physical Review Research* **6**(4), 043182 (2024)
- [107] Link, V., Tu, H.-H., Strunz, W.T.: Open quantum system dynamics from infinite tensor network contraction. *Physical Review Letters* **132**(20), 200403 (2024)
- [108] Zeng, H., Sun, X.: Quantum dynamics in multistate harmonic models using tensor-train thermofield dynamics and semiclassical mapping dynamics. *The Journal of Chemical Physics* **163**(2) (2025)
- [109] Gelß, P., Matera, S., Klein, R., Schmidt, B.: Quantum dynamics of coupled excitons and phonons in chain-like systems: Tensor train approaches and higher-order propagators. *The Journal of Chemical Physics* **162**(15) (2025)
- [110] Wang, G., Sun, Y., Yang, S., Cai, Z.: Accelerated inchworm method with tensor-train bath influence functional. *arXiv preprint arXiv:2506.12410* (2025)
- [111] Park, G., Gray, J., Chan, G.K.: Simulating quantum dynamics in two-dimensional lattices with tensor network influence functional belief propagation. *arXiv preprint arXiv:2504.07344* (2025)
- [112] Chen, Q.-C., Liu, I., Li, J.-W., Chung, C.-M., et al.: Solving the gross-pitaevskii equation with quantum tensor trains: Ground states and nonlinear dynamics. *arXiv preprint arXiv:2507.04279* (2025)
- [113] Środa, M., Inayoshi, K., Schüler, M., Shinaoka, H., Werner, P.: Predictor-corrector method based on dynamic mode decomposition for tensor-train nonequilibrium green’s function calculations. *arXiv preprint arXiv:2509.22177* (2025)

- [114] Weichselbaum, A., Verstraete, F., Schollwöck, U., Cirac, J.I., Delft, J.: Variational matrix-product-state approach to quantum impurity models. *Physical Review B—Condensed Matter and Materials Physics* **80**(16), 165117 (2009)
- [115] Holzner, A., Weichselbaum, A., Delft, J.: Matrix product state approach for a two-lead multilevel anderson impurity model. *Physical Review B—Condensed Matter and Materials Physics* **81**(12), 125126 (2010)
- [116] Ganahl, M., Thunström, P., Verstraete, F., Held, K., Evertz, H.G.: Chebyshev expansion for impurity models using matrix product states. *Physical Review B* **90**(4), 045144 (2014)
- [117] Wolf, F.A., McCulloch, I.P., Parcollet, O., Schollwöck, U.: Chebyshev matrix product state impurity solver for dynamical mean-field theory. *Physical Review B* **90**(11), 115124 (2014)
- [118] Wolf, F.A., Go, A., McCulloch, I.P., Millis, A.J., Schollwöck, U.: Imaginary-time matrix product state impurity solver for dynamical mean-field theory. *Physical Review X* **5**(4), 041032 (2015)
- [119] Ganahl, M., Aichhorn, M., Evertz, H.G., Thunström, P., Held, K., Verstraete, F.: Efficient dmft impurity solver using real-time dynamics with matrix product states. *Physical Review B* **92**(15), 155132 (2015)
- [120] Schwarz, F., Weymann, I., Delft, J., Weichselbaum, A.: Nonequilibrium steady-state transport in quantum impurity models: A thermofield and quantum quench approach using matrix product states. *Physical review letters* **121**(13), 137702 (2018)
- [121] Cao, X., Lu, Y., Hansmann, P., Haverkort, M.W.: Tree tensor-network real-time multiorbital impurity solver: Spin-orbit coupling and correlation functions in sr 2 ruo 4. *Physical Review B* **104**(11), 115119 (2021)
- [122] Kohn, L., Santoro, G.E.: Quench dynamics of the anderson impurity model at finite temperature using matrix product states: entanglement and bath dynamics. *Journal of Statistical Mechanics: Theory and Experiment* **2022**(6), 063102 (2022)
- [123] Thoenniss, J., Leroose, A., Abanin, D.A.: Nonequilibrium quantum impurity problems via matrix-product states in the temporal domain. *Physical Review B* **107**(19), 195101 (2023)
- [124] Erpenbeck, A., Lin, W.-T., Blommel, T., Zhang, L., Iskakov, S., Bernheimer, L., Núñez-Fernández, Y., Cohen, G., Parcollet, O., Waintal, X., *et al.*: Tensor train continuous time solver for quantum impurity models. *Physical Review B* **107**(24), 245135 (2023)

- [125] Kloss, B., Thoenniss, J., Sonner, M., Lerose, A., Fishman, M.T., Stoudenmire, E., Parcollet, O., Georges, A., Abanin, D.A.: Equilibrium quantum impurity problems via matrix product state encoding of the retarded action. *Physical Review B* **108**(20), 205110 (2023)
- [126] Wauters, M.M., Chung, C.-M., Maffi, L., Burrello, M.: Simulations of the dynamics of quantum impurity problems with matrix product states. *Physical Review B* **109**(11), 115101 (2024)
- [127] Ng, N., Park, G., Millis, A.J., Chan, G.K.-L., Reichman, D.R.: Real-time evolution of anderson impurity models via tensor network influence functionals. *Physical Review B* **107**(12), 125103 (2023)
- [128] Chen, R., Xu, X., Guo, C.: Grassmann time-evolving matrix product operators for quantum impurity models. *Physical Review B* **109**(4), 045140 (2024)
- [129] Eckstein, M.: Solving quantum impurity models in the non-equilibrium steady state with tensor trains. *arXiv preprint arXiv:2410.19707* (2024)
- [130] Yu, Y., Erpenbeck, A., Zgid, D., Cohen, G., Parcollet, O., Gull, E.: Inchworm tensor train hybridization expansion quantum impurity solver. *Physical Review B* **112**(8), 085120 (2025)
- [131] Kim, A.J., Werner, P.: Strong coupling impurity solver based on quantics tensor cross interpolation. *Physical Review B* **111**(12), 125120 (2025)
- [132] Rohshap, S., Ritter, M.K., Shinaoka, H., Delft, J., Wallerberger, M., Kauch, A.: Two-particle calculations with quantics tensor trains: Solving the parquet equations. *Physical Review Research* **7**(2), 023087 (2025)
- [133] Matsuura, S., Shinaoka, H., Werner, P., Tsuji, N.: Tensor cross interpolation approach for quantum impurity problems based on the weak-coupling expansion. *Physical Review B* **111**(15), 155150 (2025)
- [134] Banuls, M., Orús, R., Latorre, J., Pérez, A., Ruiz-Femenia, P.: Simulation of many-qubit quantum computation with matrix product states. *Physical Review A—Atomic, Molecular, and Optical Physics* **73**(2), 022344 (2006)
- [135] Ran, S.-J.: Encoding of matrix product states into quantum circuits of one-and two-qubit gates. *Physical Review A* **101**(3), 032310 (2020)
- [136] Yuan, X., Sun, J., Liu, J., Zhao, Q., Zhou, Y.: Quantum simulation with hybrid tensor networks. *Physical Review Letters* **127**(4), 040501 (2021)
- [137] Pan, F., Zhang, P.: Simulation of quantum circuits using the big-batch tensor network method. *Physical Review Letters* **128**(3), 030501 (2022)
- [138] Anselme Martin, B., Ayrat, T., Jamet, F., Rančić, M.J., Simon, P.: Combining

- matrix product states and noisy quantum computers for quantum simulation. *Physical Review A* **109**(6), 062437 (2024)
- [139] Smith, K.C., Khan, A., Clark, B.K., Girvin, S.M., Wei, T.-C.: Constant-depth preparation of matrix product states with adaptive quantum circuits. *PRX Quantum* **5**(3), 030344 (2024)
 - [140] Berezutskii, A., Liu, M., Acharya, A., Ellerbrock, R., Gray, J., Haghshenas, R., He, Z., Khan, A., Kuzmin, V., Lyakh, D., et al.: Tensor networks for quantum computing. *Nature Reviews Physics*, 1–13 (2025)
 - [141] Cirac, J.I., Sierra, G.: Infinite matrix product states, conformal field theory, and the haldane-shastry model. *Physical Review B—Condensed Matter and Materials Physics* **81**(10), 104431 (2010)
 - [142] Milsted, A., Haegeman, J., Osborne, T.J.: Matrix product states and variational methods applied to critical quantum field theory. *Physical Review D—Particles, Fields, Gravitation, and Cosmology* **88**(8), 085030 (2013)
 - [143] Banuls, M.C., Cichy, K., Cirac, J.I., Jansen, K., Saito, H.: Matrix product states for lattice field theories. *arXiv preprint arXiv:1310.4118* (2013)
 - [144] Buyens, B., Haegeman, J., Van Acoleyen, K., Verschelde, H., Verstraete, F.: Matrix product states for gauge field theories. *Physical review letters* **113**(9), 091601 (2014)
 - [145] Kapustin, A., Turzillo, A., You, M.: Topological field theory and matrix product states. *Physical Review B* **96**(7), 075125 (2017)
 - [146] Kapustin, A., Turzillo, A., You, M.: Spin topological field theory and fermionic matrix product states. *Physical Review B* **98**(12), 125101 (2018)
 - [147] Núñez Fernández, Y., Jeannin, M., Dumitrescu, P.T., Kloss, T., Kaye, J., Parcollet, O., Waintal, X.: Learning feynman diagrams with tensor trains. *Physical Review X* **12**(4), 041018 (2022)
 - [148] Ishida, H., Okada, N., Hoshino, S., Shinaoka, H.: Low-rank quantics tensor train representations of feynman diagrams for multiorbital electron-phonon models. *Physical Review Letters* **135**(4), 046502 (2025)
 - [149] Wendland, H.: *Numerical Linear Algebra: An Introduction*. Cambridge Texts in Applied Mathematics. Cambridge University Press, Cambridge (2017). <https://doi.org/10.1017/9781316544938>
 - [150] Tang, X., Ying, L.: Wavelet-based density sketching with functional hierarchical tensor. *arXiv preprint arXiv:2502.20655* (2025)

- [151] Oseledets, I.V.: Tensor-train decomposition. *SIAM Journal on Scientific Computing* **33**(5), 2295–2317 (2011)
- [152] Fischer, S., Steinwart, I.: Sobolev norm learning rates for regularized least-squares algorithms. *Journal of Machine Learning Research* **21**(205), 1–38 (2020)
- [153] Tsybakov, A.B.: Introduction to nonparametric estimation, 2009. URL <https://doi.org/10.1007/b13794>. Revised and extended from the **9**(10) (2004)
- [154] Cai, T., Kim, D., Wang, Y., Yuan, M., Zhou, H.H.: Optimal large-scale quantum state tomography with pauli measurements. *The Annals of Statistics* **44**(2), 682–712 (2016)
- [155] Barthel, T., Lu, J.: Fundamental limitations for measurements in quantum many-body systems. *Physical Review Letters* **121**(8), 080406 (2018)
- [156] Lowe, A., Nayak, A.: Lower bounds for learning quantum states with single-copy measurements. *ACM Transactions on Computation Theory* **17**(1), 1–42 (2025)
- [157] Soleimanifar, M., Wright, J.: Testing matrix product states. In: *Proceedings of the 2022 Annual ACM-SIAM Symposium on Discrete Algorithms (SODA)*, pp. 1679–1701 (2022). SIAM
- [158] Chen, S., Gong, W., Ye, Q., Zhang, Z.: Stabilizer bootstrapping: A recipe for efficient agnostic tomography and magic estimation. In: *Proceedings of the 57th Annual ACM Symposium on Theory of Computing*, pp. 429–438 (2025)
- [159] Bakshi, A., Bostanci, J., Kretschmer, W., Landau, Z., Li, J., Liu, A., O’Donnell, R., Tang, E.: Learning the closest product state. In: *Proceedings of the 57th Annual ACM Symposium on Theory of Computing*, pp. 1212–1221 (2025)